ARTICLE

A dysregulated sebum–microbial metabolite–IL-33 axis initiates skin inflammation in atopic dermatitis

Zhuoqiong Qiu[1], Zhenlai Zhu[2], Xiaochun Liu[3], Baichao Chen[2,4], Huibin Yin[1], Chaoying Gu[1], Xiaokai Fang[3], Ronghui Zhu[1], Tianze Yu[1], Wenli Mi[5], Hong Zhou[6], Yufeng Zhou[7], Xu Yao[3], and Wei Li[1]

Microbial dysbiosis in the skin has been implicated in the pathogenesis of atopic dermatitis (AD); however, whether and how changes in the skin microbiome initiate skin inflammation, or vice versa, remains poorly understood. Here, we report that the levels of sebum and its microbial metabolite, propionate, were lower on the skin surface of AD patients compared with those of healthy individuals. Topical propionate application attenuated skin inflammation in mice with MC903-induced AD-like dermatitis by inhibiting IL-33 production in keratinocytes, an effect that was mediated through inhibition of HDAC and regulation of the AhR signaling pathway. Mice lacking sebum spontaneously developed AD-like dermatitis, which was improved by topical propionate application. A proof-of-concept clinical study further demonstrated the beneficial therapeutic effects of topical propionate application in AD patients. In summary, we have uncovered that the dysregulated sebum–microbial metabolite–IL-33 axis might play an initiating role in AD-related skin inflammation, thereby highlighting novel therapeutic strategies for the treatment of AD.

Introduction

Atopic dermatitis (AD) is a common inflammatory skin disease with a lifetime prevalence of ≤20% and manifested as intensive itch, eczematous dermatitis, and dry skin (Kennedy et al., 2018; Weidinger and Novak, 2016). Research to date has demonstrated that AD is a complex, multifactorial disease characterized by type 2 inflammatory cell infiltration, which is often induced by IL-33 and thymic stromal lymphopoietin (TSLP) produced by keratinocytes (Weidinger and Novak, 2016; Kennedy et al., 2018; Brunner et al., 2018; Werfel et al., 2016); however, the exact mechanism underlying the pathogenesis of AD, especially the initiation step, remains unclear. It is increasingly recognized that the skin microbiota are involved in the pathogenesis of AD. In AD patients, skin dysbiosis mainly manifests as decreased microbial diversity, increased abundance of the genus *Staphylococcus*, and decreased abundance of the genus *Cutibacterium* (formerly known as *Propionibacterium*; Paller et al., 2019; Li et al., 2019; Dainichi et al., 2018). Significant alterations in the metabolism of skin microbiota, such as attenuated tryptophan metabolism, are also observed in AD patients (Yu et al., 2019; Chng et al., 2016). Whether skin inflammation is induced by skin

dysbiosis, or vice versa, has long been debated. Recent studies have shown that, in children with AD, skin microbiome dysregulation precedes the appearance of skin lesions (Kennedy et al., 2017; Meylan et al., 2017), suggesting that it is skin dysbiosis that induces skin inflammation and barrier damage in AD, and not the other way around. However, the initiating factors for skin dysbiosis and the subsequent interactions between the skin microbiota and the host in the pathogenesis of AD remain unclear.

The composition and function of the skin microbiome are primarily determined by the physical and chemical characteristics of the skin, in which the folliculosebaceous unit plays a central role (Chen et al., 2018; Oh et al., 2014; Kobayashi et al., 2019). The skin microbiome is heavily influenced by the function of sebaceous glands (Baurecht et al., 2018; Kobayashi et al., 2019). The abundance of lipophilic microbes, such as *Corynebacteria* and *Cutibacteria*, is significantly correlated with the level of skin sebum, especially fatty acids (Baurecht et al., 2018). Early studies reported that AD patients have fewer and smaller sebaceous glands (Shi et al., 2015) and lower levels of sebum

[1]Department of Dermatology, Huashan Hospital, Fudan University, Shanghai, PR China; [2]Department of Dermatology, Xijing Hospital, Fourth Military Medical University, Xi'an, PR China; [3]Department of Allergy and Rheumatology, Jiangsu Key Laboratory of Molecular Biology for Skin Diseases and STIs, Hospital for Skin Diseases, Institute of Dermatology, Chinese Academy of Medical Sciences and Peking Union Medical College, Nanjing, PR China; [4]Department of Dermatology, Kaifeng People's Hospital, Kaifeng, PR China; [5]Department of Integrative Medicine and Neurobiology, School of Basic Medical Science, Institutes of Integrative Medicine, Shanghai Medical College, Fudan University, Shanghai, PR China; [6]Department of Cell Biology, School of Life Science, Anhui Medical University, Hefei, PR China; [7]Children's Hospital and Institute of Biomedical Sciences, Fudan University, Shanghai, PR China.

Correspondence to Wei Li: liweiderma@fudan.edu.cn; Xu Yao: dryao_xu@126.com.

production than healthy individuals. Moreover, these effects have been associated with decreased skin hydration (Firooz et al., 2007) and attenuated skin barrier function (Dahlhoff et al., 2016), suggesting a link between sebaceous gland dysfunction and the development of AD. Studies investigating the AD-associated skin microbiota have consistently demonstrated that, compared with healthy people, AD patients exhibit a markedly lower abundance of *Cutibacterium* species and significant alterations in lipid-related metabolism, including fatty acid metabolism and biosynthesis (Li et al., 2019). These observations suggest that the sebaceous gland–skin microbiota axis might play an unanticipated role in the pathogenesis of AD.

Abundant sebum production provides the skin microbiota with the substrates necessary for lipid metabolism, producing short-chain fatty acids (SCFAs; Chen et al., 2018; James et al., 2004). Studies have reported that SCFAs have contradictory roles in the regulation of skin homeostasis, both promoting keratinocyte inflammation through the regulation of histone deacetylase (HDAC) and attenuating skin inflammation in mouse models via the induction of regulatory T cells (Sanford et al., 2016; Schwarz et al., 2017; Keshari et al., 2019). Thus, the exact role played by SCFAs under both physiological and pathological conditions remains unclear. Additionally, no study to date has reported on the levels of SCFAs on the skin surface. In the present study, using liquid chromatography–tandem mass spectrometry (LC-MS/MS), we found that the level of propionate on the skin surface was relatively higher than that of other SCFAs and was significantly lower in AD patients than in healthy individuals, which was consistent with the observed decrease in sebum production in these patients. We further found that topical propionate application attenuated skin inflammation in mice with MC903-induced AD-like dermatitis by inhibiting IL-33 production in keratinocytes. These effects were achieved by regulating the aryl hydrocarbon receptor (AhR) signaling pathway via the inhibition of HDAC2 and HDAC3. *Cidea* KO mice that displayed decreased sebum production spontaneously developed AD-like dermatitis, which was ameliorated by topical propionate treatment. Moreover, in a proof-of-concept clinical trial, topical propionate administration alleviated skin inflammation in AD patients. Our results indicate that a sebum–microbial metabolite–IL-33 axis is involved in the pathogenesis of AD, possibly by playing an initiating role in the induction of skin inflammation.

Results

AD patients exhibit decreased production of sebum and its microbial metabolite, propionate

We first analyzed the sebum excretion rate (SER) in nonlesional skin of different body sites of AD patients and healthy individuals from different age groups using Sebutape patches. Associations between the SER and age were visualized using locally weighted scatterplot smoothing (LOESS) curves. The results showed that the SERs of AD patients were significantly lower than those of healthy individuals across all four sites assessed (Fig. 1, A–D). Detailed information regarding the differences in SERs between AD patients and healthy controls

according to age is presented in Table 1. The SER was also assessed using the Delfin SebumScale in a separate cohort. The results were consistent with those obtained using Sebutape patches, i.e., we found that SERs were lower in lesional and nonlesional skin of the antecubital fossa (Af) and forehead of AD patients than in the corresponding normal skin of healthy controls (Fig. 1, E and F). Moreover, the SERs of AD patients were negatively correlated with transepidermal water loss (TEWL) and disease severity (scoring atopic dermatitis [SCORAD]) and positively correlated with epidermal hydration (Fig. 1, G–I).

Next, we measured the levels of SCFAs, essential microbial metabolites of skin sebum (Chen et al., 2018; James et al., 2004), on the surface of nonlesional skin in the Af and back of AD patients and the corresponding normal skin of healthy controls using targeted metabolomics (Han et al., 2015). The results showed that propionate presented the highest level on the skin surface among the seven SCFAs analyzed. Additionally, the propionate level was significantly lower on the skin surface of AD patients than on that of healthy individuals in both the Af and back (Fig. 1 J), and the level of propionate was negatively correlated with the SCORAD and pruritus scores of the patients (Fig. 1, K and L). The level of caproate was also lower in the skin of AD patients, whereas that of isovalerate was higher (Fig. 1 J). However, there were no correlations between SCORAD or pruritus score and the level of isovalerate or caproate (data not shown). The metabolite isovalerate is usually associated with *Staphylococcus* spp. (Lam et al., 2018; Bos et al., 2013), suggesting that the higher level of this metabolite observed on the skin of AD patients might be due to the increased abundance of staphylococci (Yamazaki et al., 2017). These results were in line with those of our previous report, where we demonstrated a decreased abundance of lipophilic microbes, such as *Cutibacterium* species, and a significant alteration in skin microbiota-associated fatty acid metabolism and biosynthesis in AD patients (Li et al., 2019). These and our current findings indicated that a sebum–microbial metabolite axis might be involved in the pathogenesis of AD.

Topical propionate application attenuates MC903-induced AD-like dermatitis in mice by inhibiting IL-33 production

We next explored the role of propionate in AD, using an MC903-induced AD-like mouse model. Topical application with MC903 on the ears of BALB/c mice for 9 d resulted in apparent skin inflammation; however, when 1 mmol/liter propionate was applied 30 min after the MC903 application, considerably milder symptoms of skin inflammation were observed, as evidenced by the presence of fewer visible scales, less redness, and reduced ear thickness, compared with the AD model control (Fig. 2, A and B). H&E staining of ear sections on day 9 indicated decreased epidermal thickness and less inflammatory cell infiltration in the ears of AD mice administered propionate compared with that in ears of the AD model control (Fig. 2, C and D). The scratching frequency and level of total serum IgE were much lower in mice of the MC903 plus propionate group than those in the MC903 group (Fig. 2, E and F). We further found that the expression of various inflammatory cytokines, including IL-4, IL-5, IL-13, IL-6, IL-22, and IL-25, was significantly lower in the
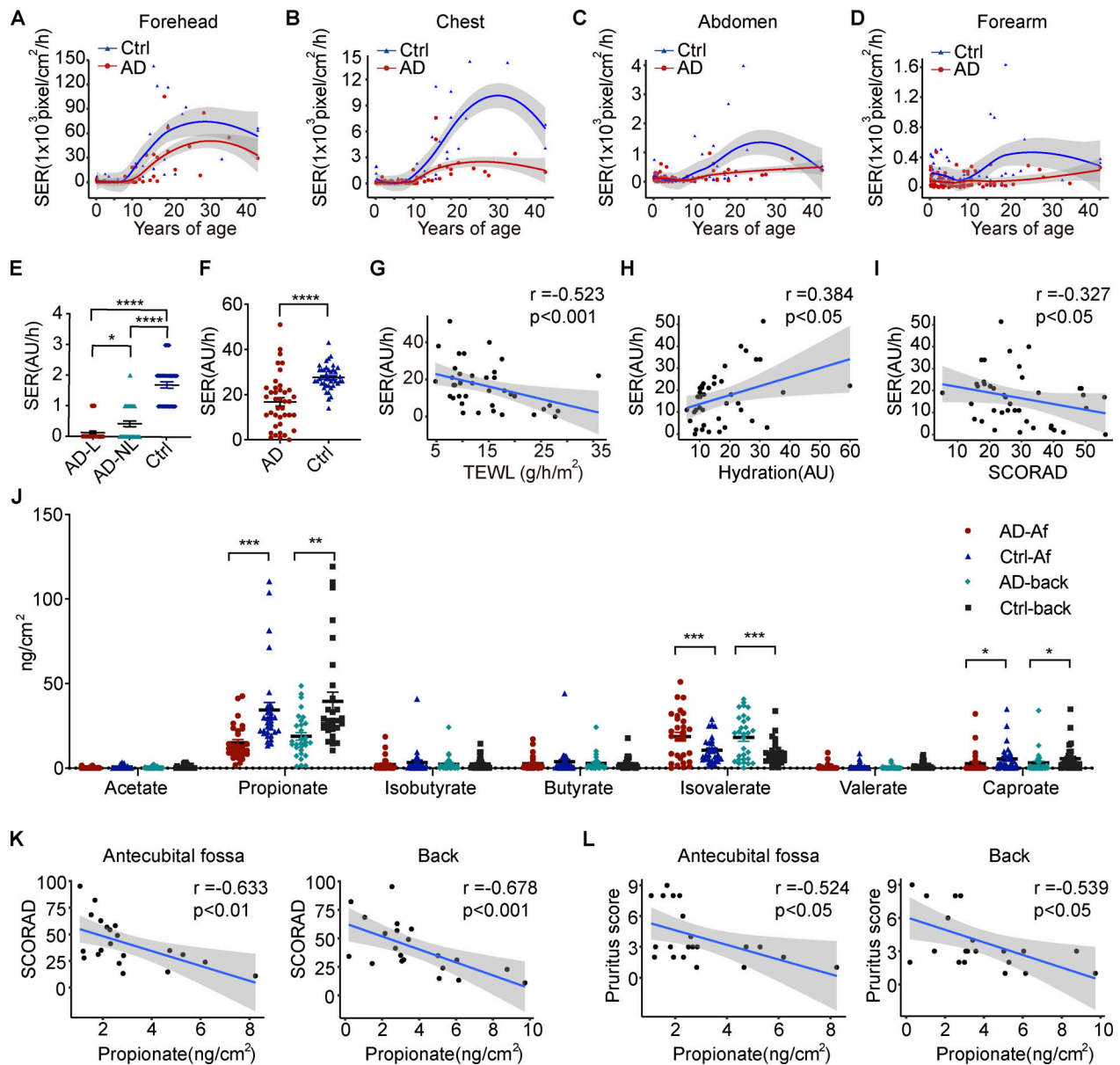
Figure 1. **The production of sebum and microbial metabolites is decreased in the skin of AD patients. (A–D)** SERs (pixels/cm²/h) measured using a Sebutape patch in nonlesional skin of different body sites of AD patients (n = 95) and healthy controls (n = 64) from different age groups. The solid lines represent LOESS fit lines. Gray shading around each line denotes 95% confidence intervals. **(E)** SERs (AU/h) measured by Delfin SebumScale in lesional (AD-L) and nonlesional (AD-NL) skin of AD patients and healthy individuals at the Af (n = 40 per group). **(F)** SERs (AU/h) measured by Delfin SebumScale in the nonlesional skin of forehead of AD patients and healthy controls (n = 40 per group). **(G–I)** Correlations between SERs and TEWL, epidermal hydration, and SCORAD of AD patients. The solid lines represent linear regression fit lines. Gray shading around each line denotes 95% confidence intervals. **(J)** SCFA levels on the nonlesional skin of the Af and the back of AD patients and healthy controls as measured by LC–MS/MS (n = 30 per group). **(K)** Correlations between the propionate level in the skin of Af/back and SCORAD of AD patients. **(L)** Correlations between the propionate level in the skin of Af/back and pruritus scores of AD patients. Data are expressed as means ± SEM. Statistical significance was analyzed by one-way ANOVA followed by Tukey's test (E), unpaired t tests with Welch's correction (F and J), and Spearman's correlation test (G–I, K, and L). *, P < 0.05; **, P < 0.01; ***, P < 0.001; ****, P < 0.0001.

ears of AD mice treated with propionate compared with that in the ears of AD model control (Fig. 2 G). As the cytokine TSLP has been implicated as the initiating factor for the skin inflammation observed in MC903-induced AD, we analyzed its expression in lesional skin using both quantitative real-time PCR (RT-qPCR) and Western blotting. We found no significant differences in TSLP expression between the propionate-treated AD mice and the AD model control (Fig. 2, H and I), indicating that TSLP

might not be involved in the attenuating effects of propionate in mice with MC903-induced dermatitis.

We then analyzed the expression of IL-33, as studies have shown that this cytokine is also required for the MC903-mediated induction of AD (Li et al., 2017; Imai et al., 2013; Molofsky et al., 2015). Immunohistochemical staining showed that IL-33 was mainly expressed in keratinocytes of the epidermis, and that IL-33 expression was markedly weaker in the

Table 1. **SERs in different body sites of AD patients and healthy controls from different age groups**

Age (yr)	Group	Forehead	Chest	Abdomen	Forearm	Total
0–2	AD (n = 31)	372.42 ± 133.71	96.13 ± 24.72	113.48 ± 22.93	88.87 ± 18.20	670.90 ± 147.59
	Control (n = 23)	1,344.52 ± 381.41	350.13 ± 111.83	158.13 ± 36.46	180.00 ± 30.17	2,032.78 ± 516.88
	P value	0.023*	0.036*	0.306	0.014*	0.018*
2–8	AD (n = 35)	386.60 ± 206.03	75.57 ± 19.36	68.46 ± 15.19	65.86 ± 10.77	596.49 ± 215.02
	Control (n = 20)	1,217.15 ± 565.01	90.55 ± 28.41	54.75 ± 6.45	135.70 ± 30.12	1,498.15 ± 569.01
	P value	0.180	0.666	0.411	0.039*	0.151
8–45	AD (n = 29)	20,666.59 ± 5,191.97	1,215.897 ± 314.13	206.7931 ± 44.89	104.069 ± 18.78	22,193.34 ± 5,309.12
	Control (n = 21)	46,844.33 ± 9,408.71	4,883.952 ± 973.13	699.4286 ± 216.26	326.381 ± 86.95	52,754.1 ± 10,299.26
	P value	0.026*	0.001**	0.036*	0.020*	0.013*

Data are expressed as means ± SEM. Statistical significance was analyzed by unpaired t test with Welch's correction. *, P < 0.05; **, P < 0.01.

propionate-treated AD mice than in the AD model control (Fig. 2 J). RT-qPCR results demonstrated that the expression level of IL-33 was significantly lower in the ears of AD mice administered propionate than in the AD model control; this result was confirmed by Western blotting (Fig. 2, K and L). We further found that propionate significantly inhibited the MC903-induced production of IL-33 in the mouse epidermal cell line JB6 (Fig. 2 M). As IL-25 from keratinocytes is also regarded as one of the initiating factors of AD inflammation, we examined the effect of propionate on IL-25 expression in JB6 cells and found that propionate had no effect on the MC903-induced production of IL-25 (Fig. 2 N), which suggested that the decreased expression of IL-25 in the ears of AD mice treated with propionate might be a downstream consequence of the overall reduced inflammation rather than a direct effect of propionate on keratinocytes.

Furthermore, we used *IL-33* KO mice and *ST2* KO mice to verify the mechanism for the antiinflammatory effect of propionate on AD mice. The results showed that AD-like inflammation induced by MC903 was significantly milder in *ST2* KO mice than in WT BALB/c mice, while propionate failed to inhibit the MC903-induced AD-like dermatitis in *ST2* KO mice (Fig. S1, A–D). When *IL-33* KO mice were used, similar phenomena were observed. AD-like inflammation was significantly milder in *IL-33* KO mice than in WT C57BL/6 mice, and propionate failed to inhibit MC903-induced AD in *IL-33* KO mice (Fig. S1, E–H). These results demonstrated the critical role of IL-33 signaling via ST2 in MC903-induced AD-like dermatitis, and the absence of *IL-33* or *ST2* abolished the propionate-mediated attenuation in skin inflammation of the MC903-treated mice. These results suggested that the inhibitory effect of propionate on AD was mainly through down-regulation of IL-33 expression. We also assessed the possibility that propionate exerts antiinflammatory effects through skin-resident immune cells such as Langerhans cells (LCs) and γδT cells. We analyzed the number of LCs and γδT cells from WT mice and *IL-33* KO mice using flow cytometry. The results showed that for WT mice, the increased numbers of both LCs and γδT cells in the MC903-induced AD model recovered after propionate application (Fig. S1, I and J), while in *IL-33* KO mice, there was no difference between the MC903 group and the MC903 plus propionate group in the numbers of LCs and

γδT cells (Fig. S1, K and L). These data suggested that the changes in the numbers of LCs and γδT cells in the WT mice group upon propionate application might be a downstream response to the changes of inflammation rather than the direct effect of propionate. Collectively, our results demonstrated that topical application of propionate attenuated MC903-induced AD-like dermatitis in mice, which might be achieved by inhibiting IL-33 expression in keratinocytes. The antiinflammatory effects of propionate were also observed in mouse models of imiquimod (IMQ)-induced psoriatic dermatitis (Fig. S2, A–D) and oxazolone (OXA)-induced contact hypersensitivity (Fig. S2, E–H).

As SCFAs have been described to be able to regulate intestinal homeostasis by inducing regulatory T cells (Tregs), we also examined whether propionate reduces AD-like inflammation by promoting Treg development in the skin. The flow cytometry results showed that the number of Tregs was increased in the lesional skin of mice in the MC903-treated group compared with the normal control (NC) group and had a tendency to recover in the MC903 plus propionate group (Fig. S2 I). RT-qPCR analysis showed that the expression of *Foxp3* and *IL-10* in mouse ears was increased in the MC903-treated group compared with the control group and returned to nearly normal levels in the MC903 plus propionate group (Fig. S2 J). These results suggested that topical application with propionate might not promote Treg development.

We also explored whether applying lipophilic microbes topically has effects similar to those of propionate. As *Cutibacterium acnes* mainly produce propionate in vitro when grown under anaerobic and lipid-rich conditions (Sanford et al., 2016), we assessed the effect of applying a mixture of *C. acnes* (1×10^5 CFU/ml) in the medium with or without 2% glycerol to mice with MC903-induced AD. The results showed that ear inflammation was significantly attenuated when the mixture of *C. acnes* and 2% glycerol was applied, as supported by fewer visible scales, less redness, and reduced ear thickness (Fig. S3, A and B). H&E staining of ear sections indicated that there were reduced epidermal thickness and less inflammatory cell infiltration in the ears of AD mice treated with the mixture of *C. acnes* and 2% glycerol compared with that in AD mice treated with *C. acnes* alone or 2% glycerol alone (Fig. S3, C and D). These data indicate
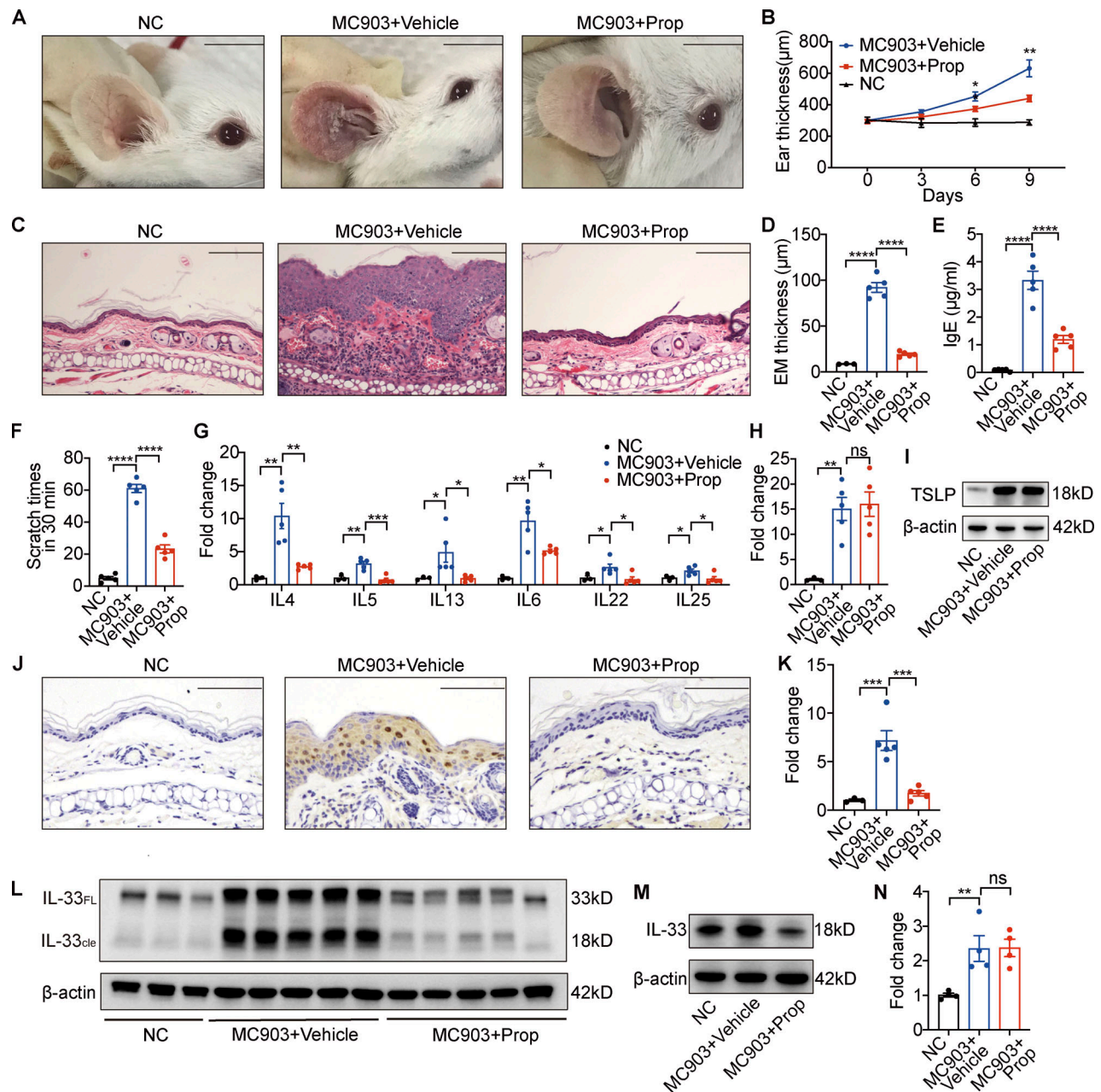
Qiu et al.   Journal of Experimental Medicine   4 of 20

Sebum–propionate–IL-33 axis in atopic dermatitis   https://doi.org/10.1084/jem.20212397

Figure 2. Topical propionate application attenuates MC903-induced AD-like dermatitis in mice by inhibiting IL-33 production. MC903 or MC903 plus propionate (Prop) was applied topically on the ears of BALB/c mice once a day for 9 d (n = 3–5 per group). **(A)** Representative gross appearance of the ears. **(B)** Dynamic changes in ear thickness on days 0, 3, 6, and 9. **(C)** H&E staining of ear sections. **(D)** Epidermal (EM) thickness of ear sections under high-power magnification. **(E)** Total serum IgE. **(F)** Scratching frequency. **(G)** mRNA expression of various cytokines in the ears of mice from each group. **(H and I)** Expression of TSLP mRNA and protein in the ears. **(J–L)** The expression of IL-33 in the ears of mice with MC903-induced AD-like dermatitis as determined by immunohistochemistry (J), RT-PCR (K), and Western blotting (L). IL-33$_{FL}$, the full-length form of IL-33; IL-33$_{cle}$, the cleaved form of IL-33. **(M)** Western blotting showing the protein expression of IL-33 in cultured JB6 cells treated with MC903 only or MC903 plus propionate. **(N)** The mRNA expression of IL-25 in cultured JB6 cells treated with MC903 only or MC903 plus propionate. Scale bar = 1 cm (A); 100 μm (C and J). Data are representative of three independent experiments and are expressed as means ± SEM. Statistical significance was analyzed by one-way ANOVA followed by Tukey's test. *, P < 0.05; **, P < 0.01; ***, P < 0.001; ****, P < 0.0001. Source data are available for this figure: SourceData F2.

that when in a lipid-rich condition, *C. acnes* could attenuate the symptoms of MC903-induced AD in mice.

Propionate inhibits IL-33 production in keratinocytes

Next, we sought to determine the effects of propionate on the production of IL-33 in human primary keratinocytes in culture.

The results showed that propionate exerted a dose-dependent inhibitory effect on IL-33 production in keratinocytes at the mRNA level (Fig. 3 A). When keratinocytes were stimulated for 1 h with proinflammatory cytokines (IL-4 and IL-1α) and then cocultured with different concentrations of propionate for 24 h, the increase in IL-33 expression was abrogated (Fig. 3 B). The
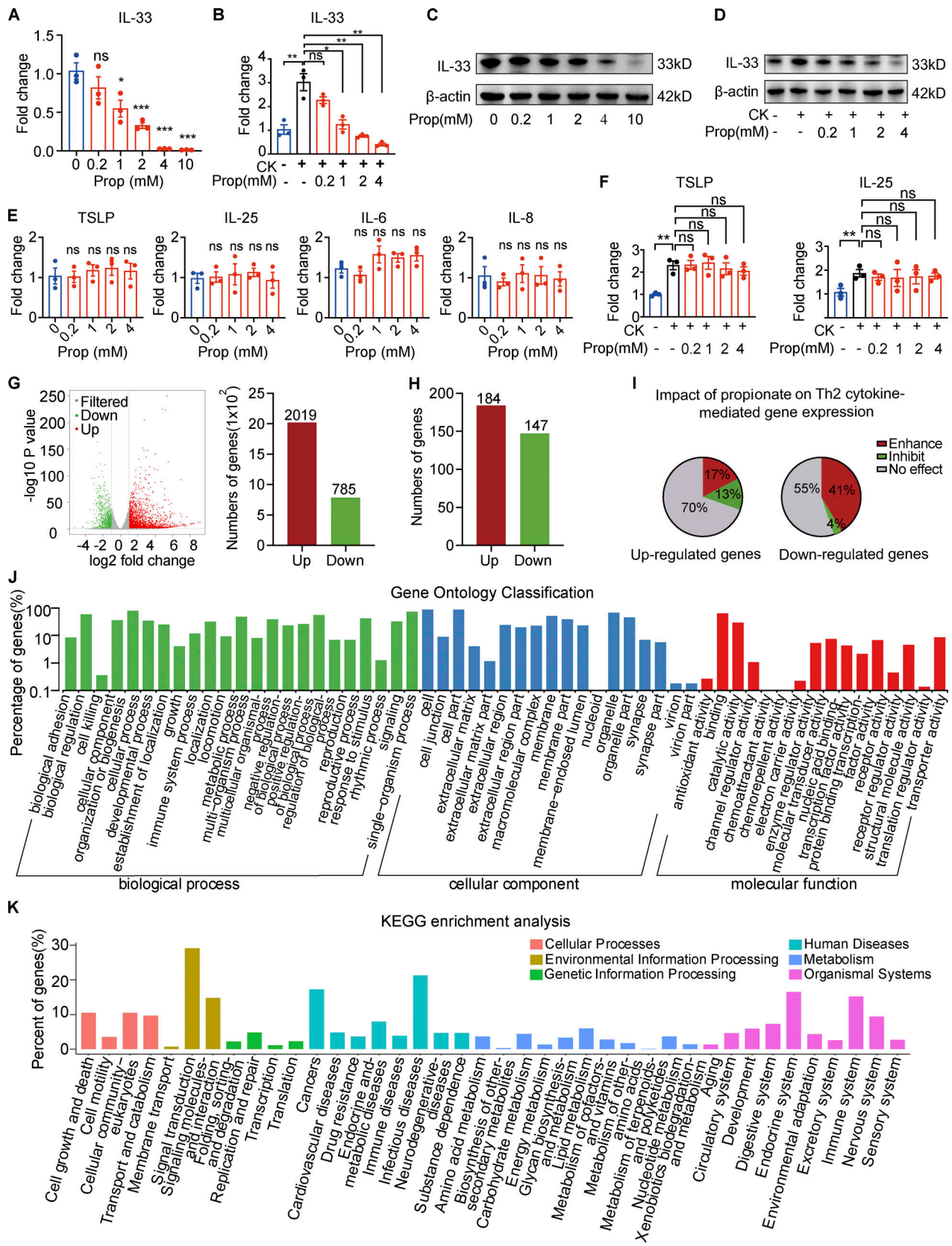
Qiu et al.
Sebum–propionate–IL-33 axis in atopic dermatitis

Journal of Experimental Medicine 5 of 20
https://doi.org/10.1084/jem.20212397

Figure 3. Propionate inhibits IL-33 production in keratinocytes. (A) RT-qPCR showing the expression of IL-33 mRNA in cultured human primary keratinocytes incubated with different concentrations of propionate for 24 h (*n* = 3 per group). **(B)** RT-qPCR showing the expression of IL-33 mRNA in cultured human primary keratinocytes stimulated with IL-4 (100 ng/ml) and IL-1α (10 ng/ml) for 1 h and then cocultured with different concentrations of propionate for 24 h (*n* = 3 per group). CK (cytokine) represents 100 ng/ml IL-4 + 10 ng/ml IL-1α. **(C)** Western blotting showing the protein expression of IL-33 in cultured

human primary keratinocytes treated with different concentrations of propionate. **(D)** Western blotting showing the protein expression of IL-33 in keratinocytes cultured under Th2 inflammatory conditions and treated with different concentrations of propionate. **(E)** RT-qPCR showing the mRNA expression of inflammatory cytokines in human primary keratinocytes incubated with different concentrations of propionate (n = 3 per group). **(F)** RT-qPCR showing the mRNA expression of inflammatory cytokines in keratinocytes cultured under Th2 inflammatory conditions and treated with different concentrations of propionate (n = 3 per group). **(G)** Volcano plots and histogram showing the DEGs (|fold-change| >2 versus control, P < 0.05) in keratinocytes treated with propionate. **(H)** DEGs (|fold-change| >2 versus control, P < 0.05) in keratinocytes stimulated with Th2 cytokines. **(I)** The effects of propionate treatment on gene sets modulated by Th2 cytokines (enhancement: fold-change >1.5 with propionate + Th2 cytokines versus vehicle + Th2 cytokines; inhibition: fold-change <−1.5 with propionate + Th2 cytokines versus vehicle + Th2 cytokines; no effect: −1.5< fold-change <1.5). **(J and K)** Gene Ontology analysis and KEGG enrichment analysis of the Th2 cytokine-induced genes in keratinocytes after propionate treatment. Data are representative of three independent experiments and are expressed as means ± SEM. Statistical significance was analyzed by one-way ANOVA followed by Dunnett's test. *, P < 0.05; **, P < 0.01; ***, P < 0.001. Source data are available for this figure: SourceData F3.

Western blotting results were in line with those of RT-qPCR (Fig. 3, C and D). Another well-studied SCFA, butyrate, also induced a dose-dependent effect on IL-33 production in keratinocytes under both steady-state and T helper cell type 2 (Th2)–mediated inflammatory conditions (Fig. S4, A–D), and the anti-inflammatory effect of butyrate was further verified in the AD mouse model induced by MC903 (Fig. S4, E–H). However, no significant changes were detected in the production of other AD-related inflammatory cytokines (IL-6, IL-8, IL-25, or TSLP) in keratinocytes following treatment with various concentrations of propionate either in the steady state or under Th2-mediated inflammatory conditions (Fig. 3, E and F). We also analyzed the effect of propionate on IL-33 production under conditions of TLR-mediated inflammation, with the results showing that propionate administration markedly abrogated the LPS (a ligand of TLR4)- or lipoteichoic acid (LTA, a ligand of TLR2)–induced increase in IL-33 expression in keratinocytes (data not shown). Collectively, these results demonstrated that propionate specifically inhibits the expression of IL-33 in human primary keratinocytes under both steady state and inflammatory conditions.

We also performed RNA sequencing (RNA-seq) analysis to comprehensively analyze the effects of propionate on keratinocytes. Using a fold-change cutoff of 2 compared with controls, we identified a total of 2,804 genes that were differentially expressed in keratinocytes after propionate treatment (785 downregulated and 2,019 upregulated; Fig. 3 G). Meanwhile, under Th2-mediated inflammatory conditions, we identified 184 genes that were upregulated and 147 downregulated (Fig. 3 H), almost half of which were further influenced by propionate administration (Fig. 3 I). Among the differentially expressed genes (DEGs), IL-33 was included in both the steady-state and the Th2-mediated inflammatory conditions. The Gene Ontology and KEGG enrichment analysis of these DEGs showed that propionate participated in environmental information processing, cell metabolism, and genetic information processing of keratinocytes (Fig. 3, J and K).

Propionate inhibits HDAC2 and HDAC3 in keratinocytes
As SCFAs have been shown to inhibit HDAC in immune cells such as macrophages and dendritic cells, thereby suppressing inflammatory cytokine production (Chang et al., 2014; Wang et al., 2008; Vinolo et al., 2011), we next explored whether the regulatory effects of propionate on IL-33 production in keratinocytes were mediated through HDAC inhibition. The results

demonstrated that propionate exerted a dose-dependent inhibitory effect on HDAC enzyme activity (Fig. 4 A). Propionate increased the global levels of histone H3K9 and H3K27 acetylation, marks that are commonly associated with actively transcribed regions of the genome (Fig. 4 B). Furthermore, the expression level of IL-33 was decreased, and the levels of histone acetylation were increased in keratinocytes treated with trichostatin A (TSA), a commonly used broad-spectrum HDAC inhibitor (Fig. 4 C).

We subsequently sought to identify which HDAC specifically regulates the expression of the IL33 gene in keratinocytes. For this, we first measured the relative transcript abundance of 11 HDACs in keratinocytes and found that the expression levels of HDAC1, HDAC2, HDAC3, and HDAC7 were relatively higher than those of the other seven HDACs (Fig. 4 D). When HDAC2 or HDAC3, but not HDAC1 or HDAC7, was knocked down in keratinocytes using siRNA, the IL-33 mRNA and protein levels were significantly decreased (Fig. 4, E–J). We also knocked down the expression of the genes encoding HDAC8 and HDAC9, which have been reported to promote the expression of inflammatory cytokines in keratinocytes (Sanford et al., 2016). We found that HDAC8 or HDAC9 depletion did not affect IL-33 expression (Fig. 4, K and L). Collectively, our results demonstrated that propionate inhibited IL-33 production in keratinocytes via the inhibition of HDAC2 and HDAC3.

Propionate downregulates IL-33 via the regulation of AhR
We next sought to identify the mechanism involved in the HDAC inhibition–induced downregulation of IL-33. We found that propionate treatment decreased the recruitment level of RNA polymerase II (Pol II) as well as that of its serine 5-phosphorylated (S5P) form at the IL-33 promoter in keratinocytes (Fig. 5 A). As both Pol II and S5P forms are involved in transcription initiation (Chang et al., 2014), these results indicated that propionate regulates IL-33 expression at the transcriptional level. Given that histone acetylation is associated with active gene transcription, and that chromatin immunoprecipitation (ChIP) results showed that propionate did not affect the level of H3K9 acetylation (H3K9ac) at the IL-33 promoter (Fig. 5 B), we speculated that the inhibition of HDAC activity might not directly regulate IL-33 gene transcription upon propionate treatment.

Analysis of the intersection between transcription factors predicted to bind the IL-33 promoter and the DEGs from the RNA-seq analysis identified AhR (Fig. S5, A and B), which was
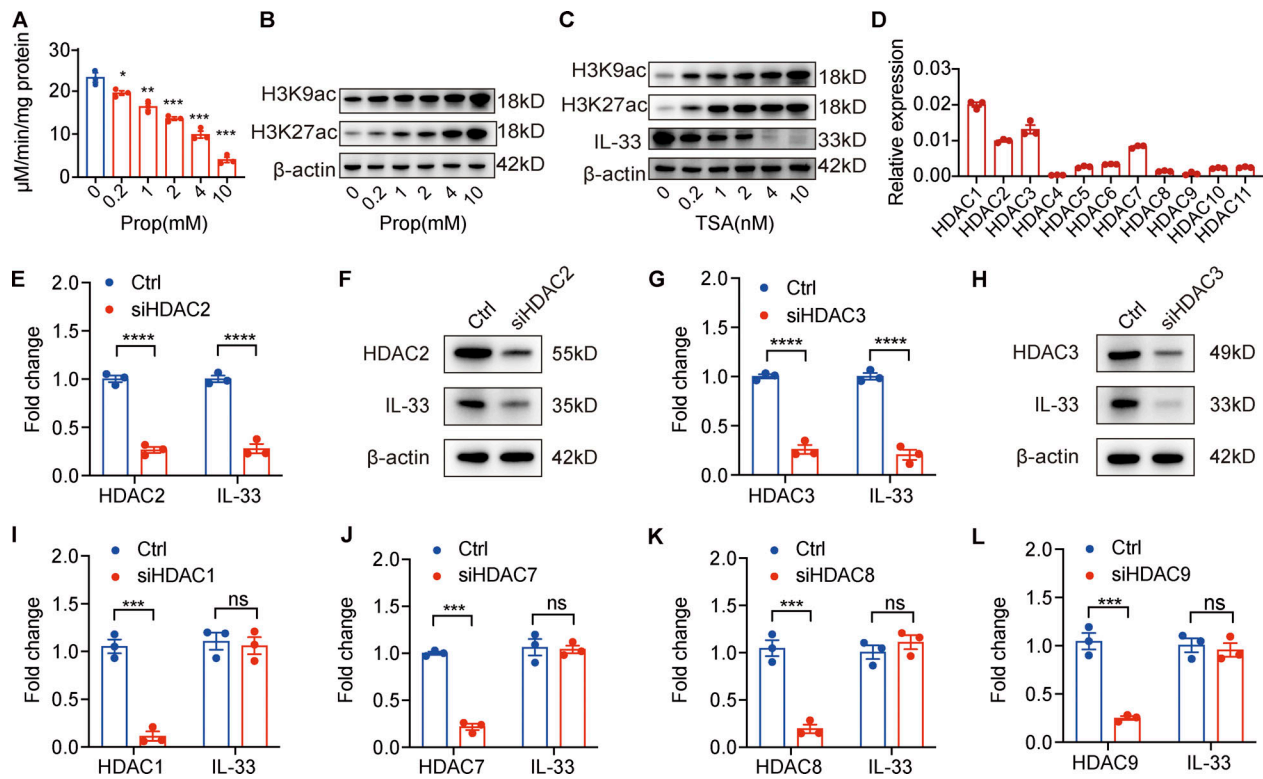
Qiu et al.
Sebum–propionate–IL-33 axis in atopic dermatitis

Journal of Experimental Medicine   7 of 20
https://doi.org/10.1084/jem.20212397

Figure 4. **Propionate suppresses IL-33 expression in human primary keratinocytes through inhibiting HDAC2 and HDAC3. (A)** HDAC enzyme activity in keratinocytes treated with different propionate (Prop) concentrations (n = 3 per group). **(B)** Western blotting showing histone acetylation in keratinocytes after treatment with different concentrations of propionate. **(C)** Western blotting of IL-33 expression and histone acetylation in keratinocytes treated with the HDAC inhibitor TSA. **(D)** The relative expression level of 11 HDACs in keratinocytes normalized to GAPDH as determined by RT-qPCR (n = 3 per group). **(E–H)** Expression of HDAC2/3 and IL-33 at the mRNA or protein level in keratinocytes after siRNA-mediated HDAC2/3 knockdown. **(I–L)** RT-qPCR results of the expression of IL-33 mRNA in keratinocytes treated with siRNA targeting HDAC1, HDAC7, HDAC8, or HDAC9. Data are representative of three independent experiments and are expressed as means ± SEM. Statistical significance was analyzed by one-way ANOVA followed by Dunnett's test (A) and unpaired t tests (E, G, and I–L; n = 3 per group). *, P < 0.05; **, P < 0.01; ***, P < 0.001; ****, P < 0.0001. Source data are available for this figure: SourceData F4.

selected for further study. As there are functional dioxin response elements for AhR binding located in the *IL-33* promoter region (Ishihara et al., 2019) and SCFAs can reportedly enhance AhR signaling (Yang et al., 2020; Jin et al., 2017; Marinelli et al., 2019), we hypothesized that the effects on IL-33 expression resulting from propionate-mediated HDAC inhibition might be exerted through enhancing AhR responsiveness. Consistent with previously reported results, we found that propionate promoted the protein expression of AhR (Fig. 5 C). We also found that TSA promoted the expression of the *AhR* gene, as well as that of the AhR-regulated genes, *CYP1A1* and *AhRR* (Fig. 5 D). Furthermore, AhR expression was significantly upregulated when either *HDAC2* or *HDAC3* was specifically silenced (Fig. 5, E and F). ChIP assay results further indicated that the level of H3K9ac at the *AhR* promoter was significantly increased after propionate treatment (Fig. 5 G). These results demonstrated that the inhibitory effect of propionate on HDAC2/3 was related to an increase in AhR expression. Fluorescence confocal microscopic analysis further showed that propionate treatment also promoted the translocation of AhR from the cytoplasm to the nucleus (Fig. 5 H), which was blocked by CH-223191, a well-characterized antagonist of the AhR-ligand binding (Fig. S5 C). Collectively, our data indicated that propionate could increase

AhR expression by inhibiting HDAC2/3 and induce AhR nuclear translocation.

We next investigated whether the inhibitory effect of propionate on IL-33 expression is dependent on AhR activation. We found that an AhR agonist, 6-formylindolo[3,2-b] carbazole, exerted an inhibitory effect similar to that of propionate on IL-33 expression in keratinocytes (Fig. 5 I), while the expression of IL-33 in keratinocytes was significantly increased when *AhR* was knocked down (Fig. 5 J). Moreover, the inhibitory effect of propionate on IL-33 expression in keratinocytes was abrogated when *AhR* was knocked down (Fig. 5 K). Additionally, no differences in gross appearance (Fig. 5 L), inflammatory cell infiltration (Fig. 5 M), and ear thickness (Fig. 5 N) were detected between *AhR* KO mice treated with MC903 and those treated with MC903 plus propionate. Propionate treatment did not suppress the increased expression of IL-33 in *AhR* KO mice treated with MC903 (Fig. 5, O and P). These results indicated that the absence of *AhR* abolished the propionate-mediated attenuation of skin inflammation in MC903-treated mice.

Furthermore, ChIP assay results showed that the binding of AhR to the *IL-33* promoter in keratinocytes was significantly increased with propionate treatment (Fig. 5 Q), while changes in AhR expression preceded that of IL-33 in propionate-treated
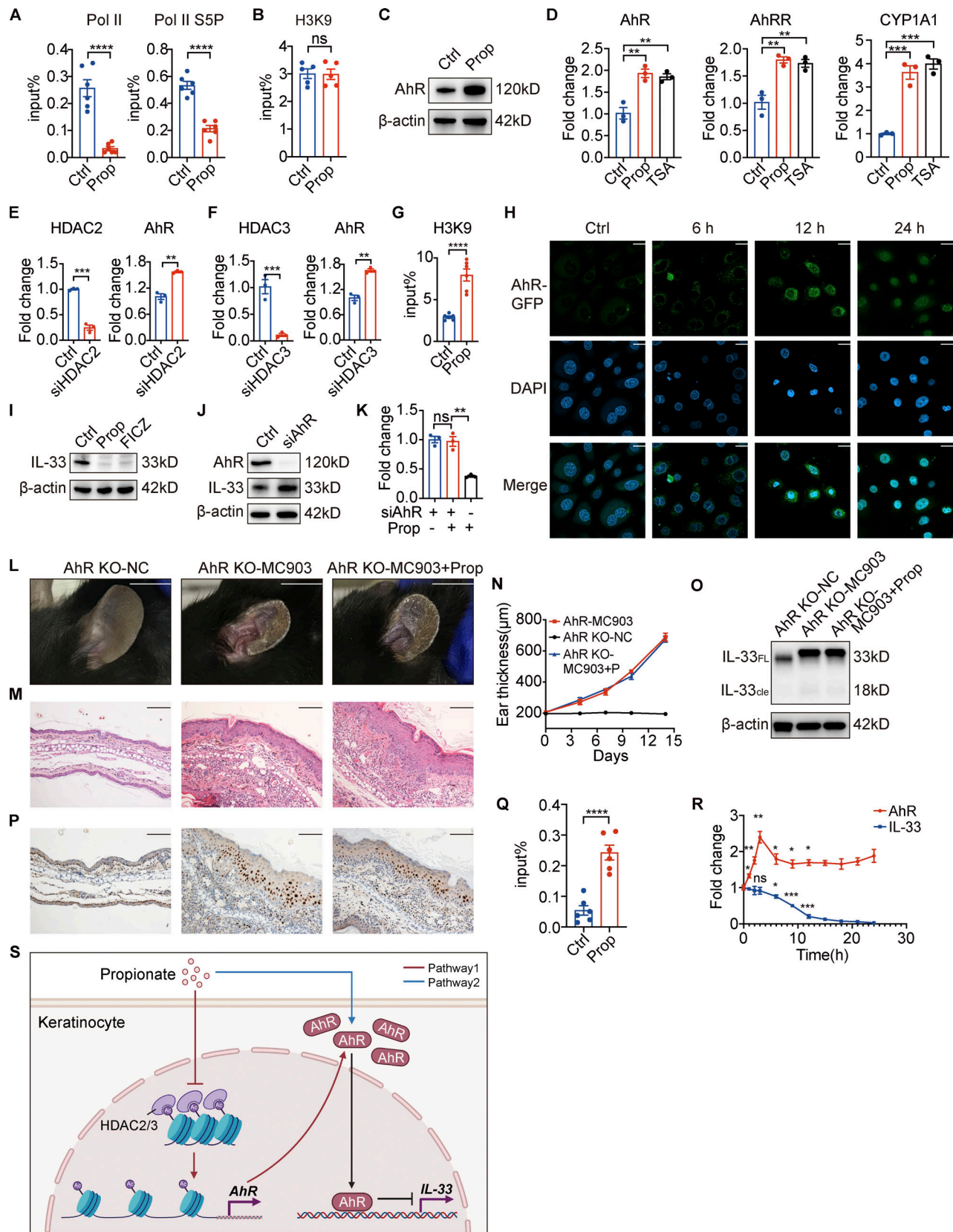
Qiu et al.
Sebum–propionate–IL-33 axis in atopic dermatitis

Journal of Experimental Medicine   8 of 20
https://doi.org/10.1084/jem.20212397

Figure 5. **Propionate induces an increase in AhR expression and facilitates its recruitment to the *IL-33* promoter. (A)** A ChIP assay was used to assess the recruitment levels of polymerase II (Pol II) and its serine 5-phosphorylated form (Pol II S5P) to the *IL-33* promoter in keratinocytes treated with propionate (Prop; *n* = 6 per group). **(B)** The levels of histone 3 lysine 9 acetylation (H3K9Ac) in the *IL-33* promoter in keratinocytes treated with propionate as determined using a ChIP assay (*n* = 6 per group). **(C)** Western blotting of the protein expression of AhR in keratinocytes treated with propionate. **(D)** RT-qPCR analysis of

the mRNA expression of AhR, AhRR, and CYP1A1 in keratinocytes treated with propionate or TSA (n = 3 per group). **(E and F)** RT-qPCR analysis of AhR mRNA expression levels in keratinocytes treated with siRNA specific for HDAC2 or HDAC3 (n = 3 per group). **(G)** A ChIP assay was used to measure the levels of H3K9Ac at the *AhR* promoter in keratinocytes treated with propionate (n = 6 per group). **(H)** Representative confocal images showing the localization of AhR in keratinocytes treated with propionate for different durations. **(I)** Western blotting analysis of the protein expression of IL-33 in keratinocytes treated with propionate or 6-formylindolo[3,2-b] carbazole (FICZ). **(J)** Western blotting analysis of the protein expression of IL-33 in keratinocytes treated with AhR-specific siRNA. **(K)** RT-qPCR analysis of IL-33 mRNA expression in keratinocytes treated with or without propionate when *AhR* was specifically silenced (n = 3 per group). **(L–P)** *AhR* KO mice with MC903-induced AD-like dermatitis were topically treated with propionate (n = 3 per group). Gross appearance (L), H&E staining of ear sections on day 14 (M), dynamic changes in ear thickness (N), Western blotting for IL-33 protein expression (O), and immunohistochemical staining of IL-33 in ear sections (P) are shown. **(Q)** The levels of AhR recruitment to the *IL-33* promoter in keratinocytes following propionate treatment were assessed by ChIP assay (n = 6 per group). **(R)** RT-qPCR analysis of AhR and IL-33 mRNA levels in keratinocytes treated with propionate at different times (n = 3 per group). **(S)** A schematic figure showing the pathway through which propionate regulates IL-33. Pathway 1 (the red lines) reflects that propionate increases AhR expression by inhibiting HDAC2/3. Pathway 2 (the blue line) reflects that propionate induces AhR nuclear translocation. The black lines reflect that increased recruitment of AhR on the *IL-33* promoter leads to IL-33 transcriptional repression. The schematic figure was created with BioRender.com. Scale bar = 20 μm (H); 1 cm (L); 100 μm (M and P). Data are representative of three independent experiments and are expressed as means ± SEM. Statistical significance was analyzed using unpaired *t* tests (A, B, E–G, and Q) and one-way ANOVA followed by Dunnett's test (D, K, and R). *, $P < 0.05$; **, $P < 0.01$; ***, $P < 0.001$; ****, $P < 0.0001$. Source data are available for this figure: SourceData F5.

keratinocytes (Fig. 5 R). Collectively, these data revealed that the effect of propionate on IL-33 production was achieved via two pathways of regulation on AhR. A schematic figure showing the regulation of IL-33 by propionate was shown in Fig. 5 S.

Previous studies have shown that several membrane-bound G protein–coupled receptors (GPCRs) in the gut act as receptors for SCFAs and have attributed some of SCFAs' effects to the activation of these GPCRs (Brown et al., 2003; Kim et al., 2013; Singh et al., 2014). We incubated keratinocytes with the Gαi-subunit inhibitor, Pertussis toxin (PTX, 0.2 μg/ml), for 1 h prior to the stimulation with propionate for 24 h. Both the results of qRT-PCR and Western blotting showed that PTX failed to abrogate the inhibitory effect of propionate on the expression of IL-33 in keratinocytes (Fig. S5, D and E). Additionally, Sanford et al. have shown that the expression levels of GPR41, GPR43, and GPR109a were extremely low in cultured epidermal keratinocytes (Sanford et al., 2016). Collectively, these data suggested that GPCRs might not be involved in the inhibition of IL-33 expression by propionate.

Sebum-deficient mice spontaneously develop AD-like dermatitis

Cidea is highly expressed in sebaceous glands (Wang et al., 2012) and is a crucial regulator of lipid storage and sebum lipid secretion in mammals, including humans (Zhang et al., 2014). We have previously shown that sebum levels on the skin surface of *Cidea* KO mice are markedly lower than those of WT controls, as are the contents of the constituents of sebum lipids, including triglycerides, wax diesters, diglycerides, phospholipids, and phosphatidylcholine (Zhang et al., 2014). In this study, we found that *Cidea* KO mice spontaneously developed AD-like dermatitis characterized by dry skin, hair loss, skin redness, scales, and scratches (Fig. 6 A). These mice also demonstrated significantly higher TEWL, lower levels of epidermal hydration, higher serum concentrations of total IgE, and higher scratching frequency than WT controls (Fig. 6, B–E).

We further assessed SCFA levels on the skin surface of *Cidea* KO mice and found that the acetate, propionate, butyrate, isovalerate, and valerate contents were significantly lower in *Cidea* KO mice than in WT controls (Fig. 6 F). However, when we applied propionate topically on the lesional skin of *Cidea* KO

mice twice daily, we found that dermatitis symptoms in the treated areas were alleviated after 21 d of application (Fig. 6, G and H). The curative effects of propionate were further confirmed by H&E staining of sections of propionate-treated lesional skin obtained from *Cidea* KO mice, as evidenced by a reduction in inflammatory cell infiltration (Fig. 6 I). Propionate ameliorated the increased level of IL-33 expression in the lesional skin of *Cidea* KO mice (Fig. 6 J). Butyrate also exhibited an inhibitory effect on the spontaneous skin inflammation of *Cidea* KO mice (Fig. S4, I–K). Combined, these results demonstrated that sebum from sebaceous glands might play a key role in the pathogenesis of AD through the microbial metabolites.

Topical propionate application ameliorates skin lesions in AD patients

To explore the effect of propionate on patients with AD, we enrolled 11 patients with mild to moderate AD and topically applied a cream containing 0.05% propionate or vehicle onto their skin lesions of symmetrical parts twice daily. After 2 wk of the treatment, dermatitis of the propionate-treated regions in the AD patients exhibited a significant improvement compared with the vehicle-treated regions (Fig. 7 A). The enrolled AD patients presented decreased skin symptom intensity and less subjective pruritus of the propionate-treated regions measured by SCORAD criteria (Fig. 7, B and C). The regional SCORAD (sum of local intensity and pruritus scores) after topical propionate treatment was also decreased (Fig. 7 D). The regional skin of AD patients with topical propionate exhibited decreased TEWL and increased skin hydration after 2 wk of treatment (Fig. 7, E and F). These results demonstrated that topical propionate application could alleviate AD symptoms in patients, suggesting a new strategy for AD treatment.

Discussion

The interaction between the skin microbiota and the host is crucial for the maintenance of skin homeostasis (Rooks and Garrett, 2016; Shapiro et al., 2014; Flowers and Grice, 2020). Various studies have reported that skin dysbiosis is involved in the pathogenesis of AD (Kennedy et al., 2018; Brunner et al., 2018; Weidinger and Novak, 2016); however, whether and
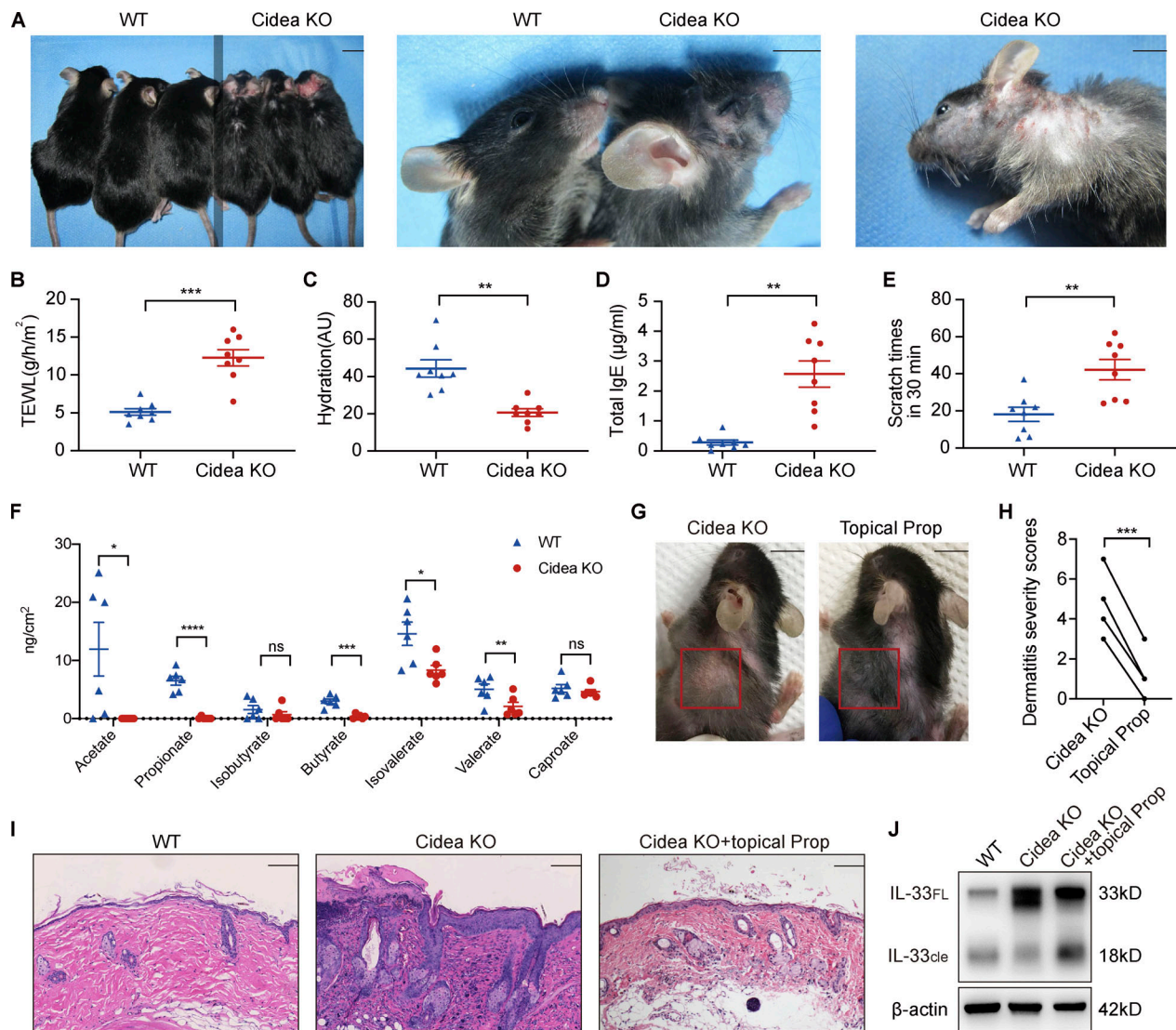
Qiu et al.
Sebum–propionate–IL-33 axis in atopic dermatitis

Journal of Experimental Medicine   10 of 20
https://doi.org/10.1084/jem.20212397

Figure 6. **Propionate attenuates spontaneous AD-like dermatitis in sebum-deficient mice. (A)** Gross appearance of skin lesions in *Cidea* KO and WT mice. The line down the middle of this panel is used to divide the two types of mice. **(B–E)** TEWL (B), epidermal hydration (C), total serum IgE (D), and scratching frequency (E) in *Cidea* KO and WT mice (*n* = 8 per group). **(F)** SCFA levels on the skin surface of *Cidea* KO and WT mice (*n* = 6 per group). **(G)** Gross appearance of skin lesions in *Cidea* KO mice before and after topical propionate treatment. The red box indicates the skin lesions treated with propionate. **(H)** The severity scores of skin lesions in *Cidea* KO mice before and after propionate treatment (*n* = 4). **(I)** H&E staining of skin samples from WT mice, lesional skin of *Cidea* KO mice, and lesional skin of *Cidea* KO mice treated with propionate. **(J)** Western blotting showing the protein expression of IL-33 in skin samples of WT mice, lesional skin of *Cidea* KO mice, and lesional skin of *Cidea* KO mice treated with propionate (Prop). Scale bar = 1 cm (A and G); 100 μm (I). Data are representative of three independent experiments and are expressed as means ± SEM. Statistical significance was analyzed by unpaired *t* test with Welch's correction (B–F) and paired *t* test (H). *, $P < 0.05$; **, $P < 0.01$; ***, $P < 0.001$; ****, $P < 0.0001$. Source data are available for this figure: SourceData F6.

how changes in the skin microbiome initiate skin inflammation, or whether it is skin inflammation that promotes changes in the composition of the skin microbiome, remains poorly understood. In the present study, we focused on the significance of decreased sebum production and its microbial metabolite, propionate, in AD patients to elucidate whether the skin microbiome has an initiating role in AD pathogenesis. Using LC-MS/MS, we detected a substantial amount of propionate on the skin surface and found that the propionate content was significantly lower in AD patients than in healthy individuals. Topical propionate application attenuated skin inflammation in mice with MC903-induced AD by inhibiting IL-33 production, an effect

that was mediated through HDAC inhibition and AhR activation. This is the first study to report on the role of SCFAs in skin homeostasis based on the determination of SCFA levels on the skin surface, with the results showing that the sebum–microbial metabolite–IL-33 axis might play an essential role in the initiation of AD-related skin inflammation.

SCFAs, produced by the fermentation of nondigestible polysaccharides in the diet, are the most studied microbial metabolites in the gut (Rooks and Garrett, 2016; Levy et al., 2017). In contrast, the importance of SCFAs in skin homeostasis has long been overlooked, as the skin surface is almost devoid of polysaccharides (Chen et al., 2018); however, the pilosebaceous unit
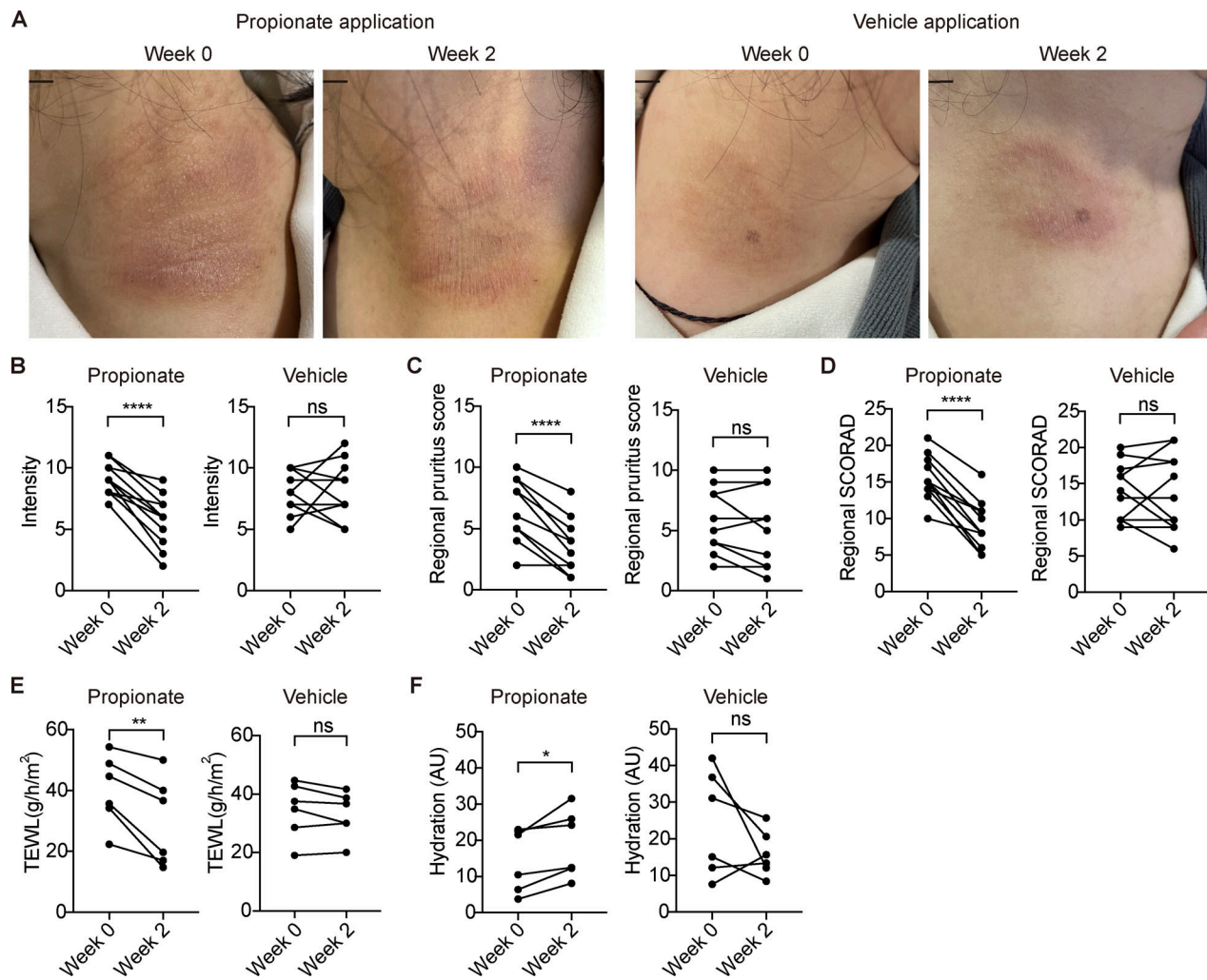
Qiu et al.
Sebum–propionate–IL-33 axis in atopic dermatitis

Journal of Experimental Medicine 11 of 20
https://doi.org/10.1084/jem.20212397

Figure 7. **Topical propionate application ameliorates the symptoms of AD patients. (A)** Representative photographs of symmetrical lesions in AD patients at enrollment (week 0) and week 2 after topical propionate or vehicle application. Scale bar = 1 cm. **(B–D)** Before- and after-treatment scores for skin symptom intensity (B), subjective pruritus (C), and treated region-specific SCORAD (D) of the propionate- or vehicle-treated region as measured by SCORAD protocol (n = 11). Treated region-specific SCORAD score is the sum of skin symptom intensity and pruritus scores. **(E and F)** Before- and after-treatment levels of TEWL (E) and skin hydration (F) of the propionate- or vehicle-treated region in enrolled AD patients (n = 6). Statistical significance was analyzed using paired t test. *, $P < 0.05$; **, $P < 0.01$; ****, $P < 0.0001$.

provides an abundance of sebum that can serve as a substrate for skin microbiota–mediated lipid metabolism, which results in the production of SCFAs (Chen et al., 2018; Byrd et al., 2018; James et al., 2004). This is the first study to properly quantify the levels of SCFAs on the skin surface. Subsequently, we uncovered that the propionate level is significantly lower in the skin of AD patients compared with healthy individuals, which is consistent with reduced sebum production, a decreased abundance of C. acnes, and alterations in microbial lipid metabolism in the skin of AD patients (Li et al., 2019; Shi et al., 2015; Chng et al., 2016). Cutibacterium is the most abundant genus in the skin, and the pilosebaceous unit contains a substantially higher level of sebum and Cutibacterium than the skin surface (Byrd et al., 2018); thus, the actual level of SCFAs in the skin should be higher than reported in this study.

In our study, the importance of sebum and propionate in the development of AD was first demonstrated by the propionate-mediated amelioration of AD-like dermatitis in mice with MC903, an effect that was further confirmed by topical propionate application in sebum-deficient Cidea KO mice which spontaneously developed AD-like dermatitis. Previous studies have shown that propionate suppresses the growth of Staphylococcus aureus both in vitro and in vivo (Shu et al., 2013; Wang et al., 2014). Consequently, the decreased levels of C. acnes and its metabolite propionate in AD patients may lead to an increase in the abundance of S. aureus in the skin of these patients. We also demonstrated that topical C. acnes application effectively alleviated AD-like dermatitis in mouse models. Considering that C. acnes helps maintain the pH of the skin (Youn et al., 2013) and promotes the expression of filaggrin and antimicrobial peptides in keratinocytes (Lee et al., 2019; Ramasamy et al., 2019), we propose that C. acnes plays an essential protective role in AD and has potential as a topical probiotic for the prevention and treatment of AD. Conversely, C. acnes is traditionally considered

as pathogen in acne (Dréno et al., 2018; Ramasamy et al., 2019). The paradoxical regulatory role of *C. acnes* between AD and acne implies that *C. acnes* might be one of the key skin commensals regulating different types of skin inflammation, which is worthy of further study. Another SCFA, butyrate, also exhibited an inhibitory effect on IL-33 production in keratinocytes. The anti-inflammatory effect of butyrate was further verified in the AD mouse model and was even stronger than that of propionate, which might be due to their differential effects on HDAC activity and AhR signaling (Silva et al., 2018; Denison and Faber, 2017). Although the level of butyrate on the skin surface was extremely low and was similar between AD patients and healthy people, butyrate's strong inhibitory effect on IL-33 expression suggests that it may also have a potential application in AD treatment. Notably, butyrate has a strong and conspicuous odor, which may hinder its use; therefore, more efforts on butyrate are needed in the future to optimize its clinical application. Besides, SCFAs have been well described to be able to modulate the number and function of colonic Tregs (Levy et al., 2017; Shapiro et al., 2014); Schwarz et al. (2017) have reported that butyrate promotes the development of Tregs in the skin of a contact hypersensitivity mouse model. However, our results suggest that Tregs might not be involved in the propionate-induced suppression of skin inflammation. The changes of Tregs in the skin of MC903-treated mice might be a downstream response to the inflammation, as previous studies have shown that the development of Tregs is affected by IL-33 (Schiering et al., 2014; Toyama et al., 2021). The discrepancy between the study of Schwarz et al. (2017) and our work may be due to the differences in inflammation types of different mouse models, observation time points, or the activity of butyrate and propionate in the two studies.

IL-33, a proinflammatory cytokine highly expressed in epithelial and endothelial cells, is often considered an upstream actor in type 2 immune responses (Molofsky et al., 2015; Cayrol and Girard, 2018) and plays a crucial role in allergic diseases via the receptor ST2, which is abundantly expressed in Th2 cells and group 2 innate lymphoid cells (Molofsky et al., 2015; Cayrol and Girard, 2018; Chan et al., 2019). The expression level of IL-33 is significantly increased in keratinocytes of the lesional skin of AD patients, and IL-33 not only acts as an initiator of the regional Th2 response in the skin (Li et al., 2017; Imai et al., 2013; Savinko et al., 2012) but also promotes gastrointestinal food allergies (Leyva-Castillo et al., 2019). Previous studies have mainly focused on the downstream effects mediated by IL-33, while the upstream regulation of IL-33 expression has been largely ignored. To our knowledge, our demonstration of the regulatory effect of SCFAs on IL-33 expression has not been previously reported. Our findings extend the range of immunomodulatory effects associated with SCFAs and hint that they may participate in diseases other than AD in which IL-33 is involved. IL-33 is constitutively expressed in cells of epithelial surfaces such as the skin, intestine, and lung and is extensively involved in the homeostasis of adipose tissue, intestine, and nerves (Cayrol and Girard, 2018; Molofsky et al., 2015; Chan et al., 2019; Leyva-Castillo et al., 2019; Savinko et al., 2012; Du et al., 2018). Additionally, as a proinflammatory factor, IL-33 is involved in the pathogenesis of various diseases such as asthma, inflammatory

bowel disease, and neurodegenerative diseases, among others (Cayrol and Girard, 2018; Molofsky et al., 2015; Chan et al., 2019; Leyva-Castillo et al., 2019; Savinko et al., 2012; Du et al., 2018). Thus, the regulatory effect of SCFAs on IL-33 may be important for maintaining the homeostasis of multiple human tissues, and IL-33 inhibition by SCFAs could be developed as a potential therapeutic strategy for the treatment of many conditions. Drugs targeting IL-33 have already been used to treat several diseases and have demonstrated high efficacy (Chen et al., 2019). Our work opens a new avenue for future study on the treatment of IL-33–related diseases. IL-25 (also known as IL-17E) not only is produced by keratinocytes, but also is derived from various immune cells, such as Th2 cells, eosinophils, and dendritic cells (Fort et al., 2001; Tang et al., 2018; Hvid et al., 2011). To our knowledge, few studies have explored the direct interactions between IL-25 and IL-33, whereas there are clues indicating that IL-33 may influence the expression of IL-25. Previous studies have shown that binding of IL-33 to the cells that express ST2 (including some immune cells and keratinocytes; Zeng et al., 2021) results in the activation of NF-κB and MAPKs (Schmitz et al., 2005), and activation of the MAPK pathway is involved in production of IL-25 (Liu et al., 2018; Zhou et al., 2017), suggesting that the expression of IL-25 might be regulated by IL-33. Besides, RNA-seq data of mouse keratinocytes show that the genes involved in IL-17 signaling pathway are upregulated by IL-33 stimulation (Zeng et al., 2021). These studies suggest that IL-33 may induce the expression of IL-25, and the decrease of IL-25 expression in the MC903 plus propionate group may be due to the decreased expression of IL-33 caused by propionate.

The mechanism underlying how IL-33 expression is regulated is poorly understood. As SCFAs are well established as HDAC inhibitors (Chang et al., 2014; Wang et al., 2008; Vinolo et al., 2011), and the inhibitory effect of propionate on HDAC enzyme activity increased in a concentration-dependent manner in our study (Fig. 5 A), we first assessed whether propionate exerted its suppressive effects on IL-33 expression in keratinocytes through the inhibition of HDACs. As SCFAs and TSA have broad-spectrum activity toward 11 HDACs, we next sought to determine which HDACs regulate IL-33 expression in keratinocytes. HDAC2 and HDAC3 were then sorted out, which is consistent with previous studies that have implicated these two HDACs in the regulation of inflammation-related gene expression in macrophages and intestinal epithelial cells (Jeong et al., 2014; Alenghat et al., 2013). Meanwhile, James et al. (2004) showed that, in keratinocytes, the inhibition of HDAC8 and HDAC9 by sodium butyrate promoted the expression of inflammatory cytokines such as IL-6, IL-8, and TNFα when stimulated by TLR ligands (Sanford et al., 2016); however, when we silenced the gene expression of HDAC8 or HDAC9, no effect on IL-33 expression was detected. Nevertheless, we observed that propionate also inhibited IL-33 expression in keratinocytes when stimulated with TLR ligands. The mechanism involved in the differential effects of propionate on the production of different inflammatory cytokines in keratinocytes requires further investigation.

The involvement of HDACs in the regulatory effects of SCFAs suggests that the skin microbiota can influence skin homeostasis

through epigenetic modifications. However, the inhibitory effect of propionate on HDACs is inconsistent with the observed inhibition of *IL-33* transcription following HDAC inhibition. HDACs are enzymes that remove acetyl groups from histones, thereby allowing the latter to bind DNA more tightly (Milazzo et al., 2020), and inhibition of HDAC activity leads to histone acetylation, resulting in transcriptional activation (Milazzo et al., 2020). Following the analysis of transcription factors predicted to bind the *IL-33* promoter and DEGs identified from our RNA-seq data, AhR was screened out. We found that propionate increased AhR expression by inhibiting HDAC2/3 and induced AhR nuclear translocation acting as a potential AhR ligand, in line with that previously reported (Marinelli et al., 2019). Additionally, we demonstrated that AhR exerts a negative regulatory effect on *IL-33* gene transcription in keratinocytes. Our previous study showed that activation of AhR by a tryptophan metabolite suppressed the expression of TSLP in MC903-mediated inflamed skin of mice, but in this study activation of AhR by propionate had no effect on the expression of TSLP. This discrepancy may be due to the nature and manner of function of AhR. Generally, AhR exists in the cytosol in an inactive form. After ligand binding, AhR translocates into the nucleus and forms a dimer with a nuclear protein called ARNT (AhR nuclear translocator). Then the AhR: ARNT heterodimer binds to a specific DNA recognition site called DRE (the dioxin responsive element) and influences the transcription of target genes (Shinde and McGaha, 2018; Denison et al., 2002; Stockinger et al., 2014). Previous studies have demonstrated that different AhR ligands may exert different effects on the same genes, which may result from ligand-specific changes in the structure of AhR, AhR: ARNT, and/or other AhR: protein complexes (Denison and Faber, 2017; Denison et al., 2011; Nault et al., 2013; Goodale et al., 2013). These complexes could interact with different subsets of transcriptional modulators, thereby inducing different responses of gene expression (Soshilov and Denison, 2008; Zhang et al., 2008). The differences in ligand-specific effects on target gene expression may account for the discrepancy in effects of propionate and the tryptophan metabolite on *TSLP* gene. Detailed mechanisms for the differential ligand responses on *TSLP* gene in human primary keratinocytes remain to be elucidated.

A limitation of our study is that we did not enroll people >45 yr of age for the SER study. Therefore, caution should be used when extending conclusions to people >45 yr of age. In addition, because of the volatile nature of SCFAs, we cannot accurately assess the actual amounts of SCFAs in the skin, which might be higher than the value we measured in this study.

In conclusion, our investigations have uncovered a sebum–microbial metabolite–IL-33 axis that initiates the skin inflammation in AD. The results of the proof-of-concept clinical study further confirmed the inhibitory effects of propionate on skin inflammation. Formally designed clinical trials should be carried out in the future. SCFAs have advantages as natural metabolites fermented by commensal microbiota, indicating a safer, more economical, and efficient strategy for the treatment of AD and other IL-33–related diseases.

Materials and methods
Subjects and SER assessments

Two cohorts applied by two methods were included for the evaluation of SER. The UK refinement of Hanifin and Rajka's criteria was applied to diagnose AD (Williams et al., 1994). Healthy subjects were defined as those without any history of allergic skin disease or systemic disease. The subjects were asked not to bathe for ≥8 h before the sampling. This study was approved by the institutional review boards (IRBs) of Xijing Hospital and Huashan Hospital, and all participants provided written informed consent. Sample size was determined on the basis of our previous study of tryptophan metabolite levels on human skin surface (Yu et al., 2019).

One cohort included 95 AD patients and 64 age- and gender-matched healthy individuals aged 1–45 yr. In this cohort, Sebutape patches (CuDerm) were applied to assess the SER as previously described (Bissonnette et al., 2015). Briefly, the SER was measured at four body sites: the forehead (0.5 cm from the upper edge of the eyebrow arch), chest (2 cm below the upper edge of the sternum), abdomen (1 cm above the umbilicus), and flexion side of the forearm (1 cm below the Af transverse lines). These test sites were first washed three times with medical gauze soaked in soapy water and then three times with 75% ethanol solution to ensure the removal of sebum remaining on the skin surface. Sebutape patches (3 × 1.5 cm) were then applied to the skin surface at each site, and the subjects were asked to remain in an environment with controlled temperature (23 ± 1°C) and relative humidity (50 ± 10%). After 1 h, the Sebutape patches were peeled off and applied onto a black plastic card, scanned with a CanoScan LiDE300 scanner (Canon), and analyzed using Image-Pro Plus software. The SER was expressed as areas occupied by sebum per square centimeter of a Sebutape in 1 h (pixels/cm²/h). The association between SER and age was visualized as fitted smooth curves with confidence regions using the R function LOESS.

The other cohort included 40 AD patients and 40 age- and gender-matched healthy individuals. Here, SERs were measured using the Delfin SebumScale (Delfin Technologies) at two body sites (antecubital fossa and forehead), 1 h after the washing of skin as mentioned above. The SER was expressed as the amount of sebum secreted in 1 h (AU/h). TEWL was measured with a VapoMeter (Delfin Technologies), and skin hydration was measured with a MoistureMeter SC (Delfin Technologies). SCORAD values were determined under standard approaches (Kunz et al., 1997). All the tests were carried out in a room with controlled temperature (23 ± 1°C) and relative humidity (50 ± 10%).

SCFA collection and quantification

Samples for the assessment of skin SCFAs were collected from 30 AD patients and 30 age- and gender-matched healthy individuals by tape stripping. This study was approved by the Huashan Hospital IRB, and all participants provided written informed consent. The subjects were enrolled as previously described and were asked not to bathe for ≥8 h before the sampling. The patients provided subjective values (score 0–10) for pruritus scores. A 2 × 4-cm tape (3M 810 Scotch Tape,

Qiu et al.
Sebum–propionate–IL-33 axis in atopic dermatitis

Journal of Experimental Medicine   14 of 20
https://doi.org/10.1084/jem.20212397

S-9783) was stuck on the Af and the back of subjects with the same pressure and then peeled off. The sticking and peeling cycle was repeated 20 times with the same tape on a delimited area (16 cm²) of the Af and back. For *Cidea* KO mice, tape stripping was performed as mentioned above on a shaved area (4 cm²) on the back of the mice.

The tapes were cut into small pieces with sterile scissors and collected in a 1.5-ml EP tube containing 250 µl of 50% aqueous acetonitrile, following which the tubes were vortexed (1,200 rpm) for 1 min to extract the SCFAs. The samples were then centrifuged at 12,000 rpm for 5 min at 4°C (Eppendorf), and the clear supernatants were collected. Aliquots (40 µl) of the supernatants were mixed with a solution containing 20 µl 3-nitrophenylhydrazine · HCl (200 mM), 20 µl *N*-(3-dimethyla-minopropyl)-*N*′-ethylcarbodiimide · HCl (120 mM), and 6% pyridine and incubated at 40°C for 30 min for derivatization. After the reaction, the mixtures were cooled on ice for 1 min before dilution with 320 µl of 10% aqueous acetonitrile. A 50-µl volume of this mixture was mixed with 50 µl of isotope-labeled solutions as previously described (Han et al., 2015), and a 20-µl aliquot of the final mixture was subjected to LC–MS/MS analysis. The quantification of SCFAs was performed on an Agilent 1290 LC system coupled to an Agilent 6545 quadrupole time-of-flight mass spectrometer. Chromatographic separation was performed on an Agilent ZORBAX Eclipse Plus C18 (2.1 × 100 mm, 1.8 µm) column, using water (containing 0.1% formic acid, vol/vol) and acetonitrile (containing 0.1% formic acid, vol/vol) as the mobile phase. The flow rate was 0.35 ml/min, and samples were kept at 5°C. MS data were collected as previously described (Han et al., 2015). The raw MS data were analyzed using Agilent Technologies MassHunter Workstation B.09.00 Software Quantitative Analysis. The samples were quantified in relation to SCFA standards (Dr. Ehrenstorfer) measured in parallel.

Mouse studies
WT C57BL/6 and BALB/c mice were purchased from Shanghai Slac Laboratory Animal Company. *AhR* KO mice (#002831; JAX stock) in the background of C57BL/6 were purchased from The Jackson Laboratory. *Cidea* KO mice in the background of C57BL/6 were a gift from Peng Li's laboratory (School of Life Sciences, Tsinghua University, Beijing, China; Wang et al., 2012). *IL33* KO mice in the background of C57BL/6 were provided by Dr. Hiroshi Kiyonari at the Laboratory for Animal Resources and Genetic Engineering, Center for Developmental Biology, Institute of Physical and Chemical Research, Kobe, Japan (Oboki et al., 2010). *ST*2 KO mice in the background of BALB/c were provided by Dr. Andrew McKenzie at the MRC Laboratory of Molecular Biology (Townsend et al., 2000). All KO mice had been backcrossed ≥10 times to their respective background. Corresponding WT littermates were used as controls for KO mice. All the mice used in this study were kept in sterile specific pathogen–free environments. Age- and sex-matched 6–8-wk-old mice were randomly assigned to animal studies. All animal experiments were approved by the Department of Laboratory Animal Science, Fudan University.

The MC903-induced AD-like dermatitis was performed by applying 2 nmol MC903 (calcipotriol; Leo Pharma) on mice ears for 9–14 d (9 d for WT BALB/c mice and *ST*2 KO mice; 14 d for WT

C57BL/6 mice, *IL33* KO mice, and *AhR* KO mice). IMQ-induced psoriatic dermatitis was produced by painting 5 mg IMQ cream (containing 5% IMQ; MED-SHINE) on mouse ears once daily for 7 consecutive days. The OXA–induced contact hypersensitivity was prepared by sensitizing the mice with 100 µl of 3.0% OXA (dissolved in anhydrous ethanol; Sigma-Aldrich) on the shaved abdomen and challenging them with 10 µl of 1% OXA on ears 5 d later. Three groups were set up for each mouse model: NC group, model control group, and propionate-treated group, with 3–5 mice per group. Mice in the propionate-treated group were applied with 30 µl of 1 mM sodium propionate (dissolved in a 7:3 mix solvent of 1,2-propanediol: isopropyl alcohol) topically onto ears 30 min after MC903, IMQ, or OXA application once a day; in the model control group, 30 µl of the solvent was used as the vehicle. Mice without any treatment served as the NC group. Mice in the butyrate-treated group were applied with 30 µl of 1 mM sodium butyrate (dissolved in a 7:3 mix solvent of 1,2-propanediol: isopropyl alcohol) topically onto ears 30 min after MC903 application once daily. The full thickness of mouse ears was assessed with a micrometer. Formalin-fixed and paraffin-embedded ear sections were stained with H&E or anti-mouse IL-33 antibody (Clone# EPR17831, Cat# ab187060; Abcam) for immunohistochemical staining. The fresh ear tissues were collected for RNA or protein extraction.

For testing the effect of external use of *C. acnes* on AD mouse model, *C. acnes* strain ATCC6919 was purchased from ATCC and cultured on blood agar plates (37°C, anaerobically). Age-matched BALB/c mice were randomly divided into four groups: 30 µl of 2% glycerol (glycerol control group), *C. acnes* (1 × 10⁵ CFU/ml; *C. acnes* control group), or 2% glycerol plus *C. acnes* (1 × 10⁵ CFU/ml; experimental group). Treatments were topically painted onto the ears of mice 30 min after the application with MC903, once a day for 9 consecutive days, and mice without any treatment served as the NC group.

For *Cidea* KO mice, TEWL and skin hydration were performed in compliance with that of humans as described above. The number of scratching movements recorded by video in 30 min was evaluated. Blood samples were collected for ELISA of IgE. 30 µl of 1 mM sodium propionate/butyrate (dissolved in a 7:3 mix solvent of 1,2-propanediol:isopropyl alcohol; Schwarz et al., 2017) was applied topically on lesions of *Cidea* KO mice twice a day for 3 wk. The severity scores of AD-like lesions of mice were assessed before and after the sodium propionate treatment according to four symptoms: (1) erythema, (2) scarring/dryness, (3) edema, and (4) erosion/excoriation as described previously (Sung et al., 2018). Each symptom was scored depending on its severity: 0 = none, 1 = mild, 2 = moderate, and 3 = severe. The dermatitis severity score was the sum of these four values. The lesional tissues before and after the sodium propionate treatment were collected for histopathology assessment as described previously (Yu et al., 2019). Skin tissues were fixed in 4% paraformaldehyde, paraffin-embedded, sectioned, and stained with H&E.

Cell isolation and flow cytometry
Mice ear tissues were cut into pieces and placed in 2.5 mg/ml Dispase II (Roche) solution at 4°C overnight. Then the epidermis was torn off and digested with 0.025% trypsin at 37°C for 15 min,

Qiu et al.
Sebum–propionate–IL-33 axis in atopic dermatitis

Journal of Experimental Medicine 15 of 20
https://doi.org/10.1084/jem.20212397

and an equal volume of FBS was added. After being filtered through a 70-μm cell strainer, the cells were resuspended in PBS with 1% FBS. For detecting Tregs, mice ear tissues were cut into pieces and placed in the digestion cocktail (a solution consisting of 2 mg/ml collagenase XI [Cat# C9407; Sigma-Aldrich], 0.5 mg/ml hyaluronidase [Cat# H3506; Sigma-Aldrich], and 0.1 mg/ml DNase [Cat# D5025; Sigma-Aldrich]) with shaking at 255 rpm in 37°C for 40 min (Moreau et al., 2021). Then an equal volume of FBS was added. After being filtered through a 70-μm cell strainer, the cells were resuspended in PBS with 1% FBS. Dead cells were excluded using Fixable Viability Dye eFluor 780 (eBioscience). The single-cell suspensions were stained per the manufacturer's recommendations with anti-CD207 (Cat# 144206; BioLegend), anti-MHC II (Cat# 107605; BioLegend), anti-CD3ε (Cat# 152311; BioLegend), anti-γδ TCR (Cat# 118107; BioLegend), anti-CD3 (Cat# 152311; BioLegend), anti-CD4 (Cat# 100406; BioLegend), and anti-Foxp3 (Cat# 563101; BD Pharmingen). After washing with PBS, the cells were subjected to flow cytometry analysis (BD Fortessa II), and the data were analyzed using FlowJo v10.4.

Cell culture and stimulation

Human primary keratinocytes were isolated from normal foreskin tissues as described above (Peng et al., 2017). The normal foreskin tissues obtained from circumcisions were cut into pieces and placed in 2.5 mg/ml Dispase II (Roche) solution at 4°C overnight. Then the epidermis was torn off and digested with 0.025% trypsin for 10 min, and an equal volume of FBS was added. After being filtered through a 70-μm cell strainer, the cells were cultured with Keratinocyte Growth Medium 2 (PromoCell) in a 25-cm^2 culture flask at 37°C with 5% CO$_2$. The primary keratinocytes were incubated with different concentrations (0.2–10 mM) of sodium propionate/butyrate for 24 h or stimulated with 100 ng/ml IL-4 (R&D Systems) and 10 ng/ml IL-1α (R&D Systems) and then cocultured with sodium propionate/butyrate (0.2–4 mM) for 24 h. For siRNA-mediated gene silencing, HDACs and AhR genes were knocked down in keratinocytes using siRNA purchased from RiboBio. siRNAs were transfected into keratinocytes using RNAiMax (Invitrogen) following the manufacturer's protocol. The cells were then collected for RNA or protein extraction. The sequence for siRNAs were as follows: HDAC1 siRNA (target sequence: 5′-GCGACTGTTTGAGAACCTT-3′), HDAC2 siRNA (target sequence: 5′-GACCCATAACTTGCTGTTA-3′), HDAC3 siRNA (target sequence: 5′-GTGGTTATACTGTCCGAAA-3′), HDAC7 siRNA (target sequence: 5′-CTCACGTCCAGGTGATCAA-3′), HDAC8 siRNA (target sequence: 5′-GAAGCATATGCACTGCATA-3′), HDAC9 siRNA (target sequence: 5′-AGCCACCCTCATGTTACTT-3′), AhR siRNA (target sequence: 5′-GCACCGATGGGAAATGATA-3′), and control siRNA (5′-TTCTCCGAACGTGTCACGT-3′). JB6 cells (#CRL-2010; ATTC) cultured in DMEM containing 10% FBS were stimulated with MC903 (100 ng/ml; Sigma-Aldrich) for 1 h and then treated with or without 4 mM sodium propionate for 24 h. The cells were collected for protein extraction.

Western blotting

Western blotting was performed as described previously (Yu et al., 2019). The cells were harvested and lysed with radioimmunoprecipitation assay (RIPA) buffer (Beyotime) for protein extraction. The tissues were ground with liquid nitrogen and then lysed in RIPA buffer. The BCA Protein Assay Kit (Beyotime) was used to measure the concentrations of proteins in lysates. The protein lysates were added with 1× SDS loading buffer and denatured at 100°C for 10 min. Equal total proteins were run on 10% SDS-PAGE gel and transferred to 0.45 μm nitrocellulose membranes (Millipore Immobilon). The membranes were blocked with 5% BSA and incubated with primary antibodies against indicated targets at 4°C overnight. After being incubated with goat anti-rabbit IgG secondary antibody (cat# 7074; Cell Signaling Technology) for 1 h at room temperature, the protein blots were subjected to ECL reaction and were imaged by a TANON 5200 imaging system or a LAS 3000 imager (FujiFilm). Primary antibodies in this study included anti–IL-33 antibody (Clone# EPR20417, Cat# ab207737; Abcam; Clone# EPR17831, Cat# ab187060; Abcam), anti-TSLP antibody (rabbit polyclonal, ab188766; Abcam), anti–β-actin antibody (#4967; Cell Signaling Technology), anti-histone H3 acetyl K9 antibody (Clone# Y28, Cat# ab32129; Abcam), anti-histone H3 acetyl K27 antibody (Clone# EPR21218, Cat# ab213279; Abcam), anti-HDAC2 antibody (Clone# Y461, Cat# ab32117; Abcam), anti-HDAC3 antibody (Clone# EP462Y, Cat# ab76295; Abcam), and anti-AhR antibody (Clone# EPR7119, Cat# ab190797; Abcam).

RT-qPCR

Total RNA was extracted from cells or mouse tissues using Trizol following the manufacturer's protocol (Invitrogen, Life Technologies). The RNA was measured for concentration with a NanoDrop 2000 spectrophotometer (Thermo Fisher Scientific) and reverse-transcribed to cDNA using the PrimerScript RT Reagent Kit. RT-qPCR was performed in a QuantStudio 6Flex Real-time PCR System (Thermo Fisher Scientific) using T.B. Green Premix Ex Taq II according to the manufacturer's instructions. The analysis of relative gene expression (fold-change) was determined by ΔΔCt normalized to β-actin. The primers were listed in Table S1.

RNA-seq

Purified RNA was extracted with the mirVana miRNA Isolation Kit (Ambion). The libraries were constructed using TruSeq Stranded mRNA LTSample Prep Kit (Illumina) and sequenced on the Illumina sequencing platform (HiSeqTM 2500). Raw data were processed using Trimmomatic (Bolger et al., 2014). DEGs were identified using the DESeq R package. Gene Ontology enrichment (Huang et al., 2009) and KEGG (Kanehisa et al., 2008) pathway enrichment analysis of DEGs was performed using R based on the hypergeometric distribution.

HDAC activity assay

HDAC activity was measured with an HDAC activity colorimetric assay kit (cat# K331; Biovision) according to the manufacturer's protocol. Briefly, 100 μg of cell lysates were added with 10 μl of 10× HDAC assay buffer and 5 μg of HDAC colorimetric substrates and incubated at 37°C for 1 h. The mixture was then added with 10 μl of Lysine Developer and set at 37°C for another 30 min. The sample signals (OD values) were read in an

Qiu et al.
Sebum–propionate–IL-33 axis in atopic dermatitis

Journal of Experimental Medicine 16 of 20
https://doi.org/10.1084/jem.20212397

ELISA plate reader at 400 nm. The HDAC activity was quantified according to the standard curve measured in parallel.

ChIP

ChIP assay was determined with a SimpleChIP Enzymatic Chromatin IP Kit (cat# 9003; Cell Signaling Technology) according to the manufacturer's protocol. Briefly, cells were fixed with 1% formaldehyde and disrupted by sonication. Fragmented chromatin was incubated with anti-RNA polymerase II (phospho S5) antibody (clone# 4H8, cat# ab5408; Abcam), anti-RNA polymerase II antibody (cat# 664911; BioLegend), anti-histone H3 acetyl K9 antibody (clone# Y28, cat# ab32129; Abcam), and anti-AhR antibody (clone# EPR7119, cat# ab190797; Abcam), together with protein G magnetic beads at 4°C overnight. After magnetic beads washing, cross-links reversing, and DNA purification, qPCR was used to assess the amount of immunoprecipitated DNA by using primers listed in Table S1. The fold enrichment was calculated as 2−ΔΔCt and expressed as the percentage of the total input chromatin (input%).

AhR localization experiments

To determine the localization of AhR driven by propionate, keratinocytes were transfected with a pEGFP-C3-AhR plasmid (RiboBio) using Lipofectamine 2000 Reagent (Invitrogen) following the manufacturer's protocol. Briefly, the AhR gene was cloned into a pEGFP-C3 vector, and GFP-fusion proteins were constructed. Keratinocytes were cultured in KGM containing 1 μg/ml of pEGFP-C3-AhR plasmid and 1.5 μl/ml lipofectamine 2000 for 6 h, followed by culturing in fresh KGM for 24 h. Then the keratinocytes were stimulated with 4 mM sodium propionate for a different period (0, 6, 12, and 24 h). For AhR translocation assay using CH-223191, keratinocytes that had been transfected with plasmids were pre-treated with CH-223191 (10 μM, #C8124; Sigma-Aldrich) for 1 h, and then treated with sodium propionate (4 mM) for a different period (0, 6, 12, and 24 h), After nuclear staining with DAPI (Beyotime), confocal images of the localization of AhR in keratinocytes at different time points were taken with LSM 800 confocal microscope (Zeiss). Image processing was performed with the Zeiss Zen software (v2.6) and Adobe Photoshop software.

Clinical application of propionate

For evaluating the clinical effect of propionate application on AD patients, 11 patients with mild to moderate AD were recruited and enrolled at Huashan Hospital, Fudan University, under clinical trial no. ChiCTR2100043963 registered in Chinese Clinical Trials Registry Platform with approval from Huashan Hospital IRB. Before enrollment, all patients signed informed consent. The enrolled patients were given a cream containing 0.05% propionate or vehicle onto their skin lesions of symmetrical parts. The creams were used twice daily. Clinical characteristics of patients were assessed as described previously (Myles et al., 2018) by a blinded investigator. SCORAD values were determined under standard approaches (Kunz et al., 1997). The skin symptom intensity of the treated region was valued by dryness, erythema, edema, oozing, excoriation, and lichenification (score 0–3, respectively). The patients provided subjective values (score 0–10) for regional pruritus. The treated region-specific SCORAD score is the sum of skin symptom intensity values and pruritus scores. TEWL was measured with a VapoMeter (Delfin Technologies), and skin hydration was measured with a MoistureMeter SC (Delfin Technologies). All the tests were carried out in a room with controlled temperature (23 ± 1°C) and relative humidity (50 ± 10%).

Statistical analysis

Student's t test or Wilcoxon rank-sum test was performed to compare two groups depending on whether the data were normally distributed. Comparisons among multiple groups in this study were performed with one-way ANOVA followed by Tukey's test or Dunnett's test, which were used as described in the figure legends. The correlation between the two groups was assessed by the Spearman correlation test. All the data analysis was performed with GraphPad Prism 8.0 software. Data are presented as mean ± SEM. The following symbols were used in figures to indicate statistical significance: *, $P < 0.05$; **, $P < 0.01$; ***, $P < 0.001$; and ****, $P < 0.0001$.

Online supplemental material

Fig. S1 shows that the absence of *IL-33* or *ST2* abolishes the propionate-mediated attenuation in skin inflammation of the MC903-treated mice. Fig. S2 shows that topical propionate treatment attenuates IMQ-, OXA-, or MC903-induced skin inflammation in mice. Fig. S3 shows that lipophilic microbes cultured in lipid-rich conditions attenuate MC903-induced AD-like dermatitis in mice. Fig. S4 shows that butyrate suppresses IL-33 expression in keratinocytes and inhibits skin inflammation of AD mouse models. Fig. S5 shows the mechanism for the inhibitory effect of propionate on IL-33 expression. Table S1 lists primers for RT-qPCR analysis and ChIP assay.

Data availability

The RNA-seq data reported in this paper have been deposited in the Genome Sequence Archive in the National Genomics Data Center, Beijing Institute of Genomics (China National Center for Bioinformation), Chinese Academy of Sciences, and are publicly available as of the date of publication; accession no. GSA HRA001005 (http://bigd.big.ac.cn/gsa-human/). Any additional information required to reanalyze the data reported in this paper is available from the lead contact upon request.

Qiu et al.
Sebum–propionate–IL-33 axis in atopic dermatitis

Journal of Experimental Medicine   17 of 20
https://doi.org/10.1084/jem.20212397

for Medical Sciences (no. 2021-I2M-1-059). The graphical abstract and Fig. 5 S were created with BioRender.com.

References

Alenghat, T., L.C. Osborne, S.A. Saenz, D. Kobuley, C.G.K. Ziegler, S.E. Mullican, I. Choi, S. Grunberg, R. Sinha, M. Wynosky-Dolfi, et al. 2013. Histone deacetylase 3 coordinates commensal-bacteria-dependent intestinal homeostasis. *Nature*. 504:153–157. https://doi.org/10.1038/nature12687

Baurecht, H., M.C. Rühlemann, E. Rodríguez, F. Thielking, I. Harder, A.-S. Erkens, D. Stölzl, E. Ellinghaus, M. Hotze, W. Lieb, et al. 2018. Epidermal lipid composition, barrier integrity, and eczematous inflammation are associated with skin microbiome configuration. *J. Allergy Clin. Immunol*. 141:1668–1676.e16. https://doi.org/10.1016/j.jaci.2018.01.019

Bissonnette, R., J.E. Risch, K.J. Mcelwee, P. Marchessault, C. Bolduc, S. Nigen, and C. Maari. 2015. Changes in serum free testosterone, sleep patterns, and 5-α-reductase type I activity influence changes in sebum excretion in female subjects. *Skin Res. Technol*. 21:47–53. https://doi.org/10.1111/srt.12155

Bolger, A.M., M. Lohse, and B. Usadel. 2014. Trimmomatic: A flexible trimmer for Illumina sequence data. *Bioinformatics*. 30:2114–2120. https://doi.org/10.1093/bioinformatics/btu170

Bos, L.D.J., P.J. Sterk, and M.J. Schultz. 2013. Volatile metabolites of pathogens: A systematic review. *PLoS Pathog*. 9:e1003311. https://doi.org/10.1371/journal.ppat.1003311

Brown, A.J., S.M. Goldsworthy, A.A. Barnes, M.M. Eilert, L. Tcheang, D. Daniels, A.I. Muir, M.J. Wigglesworth, I. Kinghorn, N.J. Fraser, et al. 2003. The orphan G protein-coupled receptors GPR41 and GPR43 are activated by propionate and other short chain carboxylic acids. *J. Biol. Chem*. 278:11312–11319. https://doi.org/10.1074/jbc.M211609200

Brunner, P.M., D.Y.M. Leung, and E. Guttman-Yassky. 2018. Immunologic, microbial, and epithelial interactions in atopic dermatitis. *Ann. Allergy Asthma Immunol*. 120:34–41. https://doi.org/10.1016/j.anai.2017.09.055

Byrd, A.L., Y. Belkaid, and J.A. Segre. 2018. The human skin microbiome. *Nat. Rev. Microbiol*. 16:143–155. https://doi.org/10.1038/nrmicro.2017.157

Cayrol, C., and J.P. Girard. 2018. Interleukin-33 (IL-33): A nuclear cytokine from the IL-1 family. *Immunol. Rev*. 281:154–168. https://doi.org/10.1111/imr.12619

Chan, B.C.L., C.W.K. Lam, L.S. Tam, and C.K. Wong. 2019. IL33: Roles in allergic inflammation and therapeutic perspectives. *Front. Immunol*. 10: 364. https://doi.org/10.3389/fimmu.2019.00364

Chang, P.V., L. Hao, S. Offermanns, and R. Medzhitov. 2014. The microbial metabolite butyrate regulates intestinal macrophage function via histone deacetylase inhibition. *Proc. Natl. Acad. Sci. USA*. 111:2247–2252. https://doi.org/10.1073/pnas.1322269111

Chen, Y.E., M.A. Fischbach, and Y. Belkaid. 2018. Skin microbiota–host interactions. *Nature*. 553:427–436. https://doi.org/10.1038/nature25177

Chen, Y.L., D. Gutowska-Owsiak, C.S. Hardman, M. Westmoreland, T. MacKenzie, L. Cifuentes, D. Waithe, A. Lloyd-Lavery, A. Marquette, M. Londei, and G. Ogg. 2019. Proof-of-concept clinical trial of etokimab shows a key role for IL-33 in atopic dermatitis pathogenesis. *Sci. Transl. Med*. 11:eaax2945. https://doi.org/10.1126/scitranslmed.aax2945

Chng, K.R., A.S.L. Tay, C. Li, A.H.Q. Ng, J. Wang, B.K. Suri, S.A. Matta, N. McGovern, B. Janela, X.F.C.C. Wong, et al. 2016. Whole metagenome profiling reveals skin microbiome-dependent susceptibility to atopic dermatitis flare. *Nat. Microbiol*. 1:16106. https://doi.org/10.1038/nmicrobiol.2016.106

Dahlhoff, M., C.C. Zouboulis, and M.R. Schneider. 2016. Expression of dermcidin in sebocytes supports a role for sebum in the constitutive innate defense of human skin. *J. Dermatol. Sci*. 81:124–126. https://doi.org/10.1016/j.jdermsci.2015.11.013

Dainichi, T., A. Kitoh, A. Otsuka, S. Nakajima, T. Nomura, D.H. Kaplan, and K. Kabashima. 2018. The epithelial immune microenvironment (EIME) in atopic dermatitis and psoriasis. *Nat. Immunol*. 19:1286–1298. https://doi.org/10.1038/s41590-018-0256-2

Denison, M.S., and S.C. Faber. 2017. And now for something completely different: Diversity in ligand-dependent activation of Ah receptor responses. *Curr. Opin. Toxicol*. 2:124–131. https://doi.org/10.1016/j.cotox.2017.01.006

Denison, M.S., A. Pandini, S.R. Nagy, E.P. Baldwin, and L. Bonati. 2002. Ligand binding and activation of the Ah receptor. *Chem. Biol. Interact*. 141:3–24. https://doi.org/10.1016/S0009-2797(02)00063-7

Denison, M.S., A.A. Soshilov, G. He, D.E. Degroot, and B. Zhao. 2011. Exactly the same but different: Promiscuity and diversity in the molecular mechanisms of action of the aryl hydrocarbon (dioxin) receptor. *Toxicol. Sci*. 124:1–22. https://doi.org/10.1093/toxsci/kfr218

Dréno, B., S. Pécastaings, S. Corvec, S. Veraldi, A. Khammari, and C. Roques. 2018. Cutibacterium acnes (Propionibacterium acnes) and acne vulgaris: A brief look at the latest updates. *J. Eur. Acad. Dermatol. Venereol*. 32: 5–14. https://doi.org/10.1111/jdv.15043

Du, L.X., Y.Q. Wang, G.Q. Hua, and W.L. Mi. 2018. IL-33/ST2 pathway as a rational therapeutic target for CNS diseases. *Neuroscience*. 369:222–230. https://doi.org/10.1016/j.neuroscience.2017.11.028

Firooz, A., F. Gorouhi, P. Davari, M. Atarod, S. Hekmat, M. Rashighi-Firoozabadi, and A. Solhpour. 2007. Comparison of hydration, sebum and pH values in clinically normal skin of patients with atopic dermatitis and healthy controls. *Clin. Exp. Dermatol*. 32:321–322. https://doi.org/10.1111/j.1365-2230.2007.02364.x

Flowers, L., and E.A. Grice. 2020. The skin microbiota: Balancing risk and reward. *Cell Host Microbe*. 28:190–200. https://doi.org/10.1016/j.chom.2020.06.017

Fort, M.M., J. Cheung, D. Yen, J. Li, S.M. Zurawski, S. Lo, S. Menon, T. Clifford, B. Hunte, R. Lesley, et al. 2001. IL-25 induces IL-4, IL-5, and IL-13 and Th2-associated pathologies in vivo. *Immunity*. 15:985–995. https://doi.org/10.1016/S1074-7613(01)00243-6

Goodale, B.C., S.C. Tilton, M.M. Corvi, G.R. Wilson, D.B. Janszen, K.A. Anderson, K.M. Waters, and R.L. Tanguay. 2013. Structurally distinct polycyclic aromatic hydrocarbons induce differential transcriptional responses in developing zebrafish. *Toxicol. Appl. Pharmacol*. 272:656–670. https://doi.org/10.1016/j.taap.2013.04.024

Han, J., K. Lin, C. Sequeira, and C.H. Borchers. 2015. An isotope-labeled chemical derivatization method for the quantitation of short-chain fatty acids in human feces by liquid chromatography-tandem mass spectrometry. *Anal. Chim. Acta*. 854:86–94. https://doi.org/10.1016/j.aca.2014.11.015

Huang, D.W., B.T. Sherman, and R.A. Lempicki. 2009. Bioinformatics enrichment tools: Paths toward the comprehensive functional analysis of large gene lists. *Nucleic Acids Res*. 37:1–13. https://doi.org/10.1093/nar/gkn923

Hvid, M., C. Vestergaard, K. Kemp, G.B. Christensen, B. Deleuran, and M. Deleuran. 2011. IL-25 in atopic dermatitis: A possible link between inflammation and skin barrier dysfunction. *J. Invest. Dermatol*. 131: 150–157. https://doi.org/10.1038/jid.2010.277

Imai, Y., K. Yasuda, Y. Sakaguchi, T. Haneda, H. Mizutani, T. Yoshimoto, K. Nakanishi, and K. Yamanishi. 2013. Skin-specific expression of IL-33 activates group 2 innate lymphoid cells and elicits atopic dermatitis-like inflammation in mice. *Proc. Natl. Acad. Sci. USA*. 110:13921–13926. https://doi.org/10.1073/pnas.1307321110

Ishihara, Y., T. Haarmann-Stemmann, N.Y. Kado, and C.F.A. Vogel. 2019. Interleukin 33 expression induced by aryl hydrocarbon receptor in macrophages. *Toxicol. Sci*. 170:404–414. https://doi.org/10.1093/toxsci/kfz114

James, A.G., D. Hyliands, and H. Johnston. 2004. Generation of volatile fatty acids by axillary bacteria. *Int. J. Cosmet. Sci*. 26:149–156. https://doi.org/10.1111/j.1467-2494.2004.00214.x

Jeong, Y., R. Du, X. Zhu, S. Yin, J. Wang, H. Cui, W. Cao, and C.J. Lowenstein. 2014. Histone deacetylase isoforms regulate innate immune responses by deacetylating mitogen-activated protein kinase phosphatase-1. *J. Leukoc. Biol*. 95:651–659. https://doi.org/10.1189/jlb.1013565

Jin, U.-H., Y. Cheng, H. Park, L.A. Davidson, E.S. Callaway, R.S. Chapkin, A. Jayaraman, A. Asante, C. Allred, E.A. Weaver, and S. Safe. 2017. Short

chain fatty acids enhance aryl hydrocarbon (Ah) responsiveness in mouse colonocytes and Caco-2 human colon cancer cells. *Sci. Rep.* 7: 10163. https://doi.org/10.1038/s41598-017-10824-x

Kanehisa, M., M. Araki, S. Goto, M. Hattori, M. Hirakawa, M. Itoh, T. Katayama, S. Kawashima, S. Okuda, T. Tokimatsu, and Y. Yamanishi. 2008. KEGG for linking genomes to life and the environment. *Nucleic Acids Res.* 36:480–484. https://doi.org/10.1093/nar/gkm882

Kennedy, E.A., J. Connolly, J.O. Hourihane, P.G. Fallon, W.H.I. McLean, D. Murray, J.H. Jo, J.A. Segre, H.H. Kong, and A.D. Irvine. 2017. Skin microbiome before development of atopic dermatitis: Early colonization with commensal staphylococci at 2 months is associated with a lower risk of atopic dermatitis at 1 year. *J. Allergy Clin. Immunol.* 139:166–172. https://doi.org/10.1016/j.jaci.2016.07.029

Kennedy, K., J. Heimall, and J.M. Spergel. 2018. Advances in atopic dermatitis in 2017. *J. Allergy Clin. Immunol.* 142:1740–1747. https://doi.org/10.1016/j.jaci.2018.10.012

Keshari, S., A. Balasubramaniam, B. Myagmardoloonjin, D.R. Herr, I.P. Negari, and C.M. Huang. 2019. Butyric acid from probiotic staphylococcus epidermidis in the skin microbiome down-regulates the ultraviolet-induced pro-inflammatory IL-6 cytokine via short-chain fatty acid receptor. *Int. J. Mol. Sci.* 20:E4477. https://doi.org/10.3390/ijms20184477

Kim, M.H., S.G. Kang, J.H. Park, M. Yanagisawa, and C.H. Kim. 2013. Short-chain fatty acids activate GPR41 and GPR43 on intestinal epithelial cells to promote inflammatory responses in mice. *Gastroenterology*. 145: 396–406.e1-10. https://doi.org/10.1053/j.gastro.2013.04.056

Kobayashi, T., B. Voisin, D.Y. Kim, E.A. Kennedy, J.H. Jo, H.Y. Shih, A. Truong, T. Doebel, K. Sakamoto, C.Y. Cui, et al. 2019. Homeostatic control of sebaceous glands by innate lymphoid cells regulates commensal bacteria equilibrium. *Cell*. 176:982–997.e16. https://doi.org/10.1016/j.cell.2018.12.031

Kunz, B., A.P. Oranje, L. Labrèze, J.-F. Stalder, J. Ring, and A. Taïeb. 1997. Clinical validation and guidelines for the SCORAD index: Consensus report of the European task force on atopic dermatitis. *Dermatology*. 195: 10–19. https://doi.org/10.1159/000245677

Lam, T.H., D. Verzotto, P. Brahma, A.H.Q. Ng, P. Hu, D. Schnell, J. Tiesman, R. Kong, T.M.U. Ton, J. Li, et al. 2018. Understanding the microbial basis of body odor in pre-pubescent children and teenagers. *Microbiome*. 6: 213–214. https://doi.org/10.1186/s40168-018-0588-z

Lee, Y.B., E.J. Byun, and H.S. Kim. 2019. Potential role of the microbiome in acne: A comprehensive review. *J. Clin. Med.* 8:987. https://doi.org/10.3390/jcm8070987

Levy, M., E. Blacher, and E. Elinav. 2017. Microbiome, metabolites and host immunity. *Curr. Opin. Microbiol.* 35:8–15. https://doi.org/10.1016/j.mib.2016.10.003

Leyva-Castillo, J.M., C. Galand, C. Kam, O. Burton, M. Gurish, M.A. Musser, J.D. Goldsmith, E. Hait, S. Nurko, F. Brombacher, et al. 2019. Mechanical skin injury promotes food anaphylaxis by driving intestinal mast cell expansion. *Immunity*. 50:1262–1275.e4. https://doi.org/10.1016/j.immuni.2019.03.023

Li, C., I. Maillet, C. Mackowiak, C. Viala, F. Di Padova, M. Li, D. Togbe, V. Quesniaux, Y. Lai, and B. Ryffel. 2017. Experimental atopic dermatitis depends on IL-33R signaling via MyD88 in dendritic cells. *Cell Death Dis.* 8:e2735. https://doi.org/10.1038/cddis.2017.90

Li, W., X. Xu, H. Wen, Z. Wang, C. Ding, X. Liu, Y. Gao, H. Su, J. Zhang, Y. Han, et al. 2019. Inverse association between the skin and oral microbiota in atopic dermatitis. *J. Invest. Dermatol.* 139:1779–1787.e12. https://doi.org/10.1016/j.jid.2019.02.009

Liu, Y., Z. Shao, G. Shangguan, Q. Bie, and B. Zhang. 2018. Biological properties and the role of IL-25 in disease pathogenesis. *J. Immunol. Res.* 2018:6519465. https://doi.org/10.1155/2018/6519465

Marinelli, L., C. Martin-Gallausiaux, J.-M. Bourhis, F. Béguet-Crespel, H.M. Blottière, and N. Lapaque. 2019. Identification of the novel role of butyrate as AhR ligand in human intestinal epithelial cells. *Sci. Rep.* 9:643. https://doi.org/10.1038/s41598-018-37019-2

Meylan, P., C. Lang, S. Mermoud, A. Johannsen, S. Norrenberg, D. Hohl, Y. Vial, G. Prod'hom, G. Greub, M. Kypriotou, and S. Christen-Zaech. 2017. Skin colonization by *Staphylococcus aureus* precedes the clinical diagnosis of atopic dermatitis in infancy. *J. Invest. Dermatol.* 137:2497–2504. https://doi.org/10.1016/j.jid.2017.07.834

Milazzo, G., D. Mercatelli, G. Di Muzio, L. Triboli, P. De Rosa, G. Perini, and F.M. Giorgi. 2020. Histone deacetylases (HDACs): Evolution, specificity, role in transcriptional complexes, and pharmacological actionability. *Genes*. 11:E556. https://doi.org/10.3390/genes11050556

Molofsky, A.B., A.K. Savage, and R.M. Locksley. 2015. Interleukin-33 in tissue homeostasis, injury, and inflammation. *Immunity*. 42:1005–1019. https://doi.org/10.1016/j.immuni.2015.06.006

Moreau, J.M., M.O. Dhariwala, V. Gouirand, D.P. Boda, I.C. Boothby, M.M. Lowe, J.N. Cohen, C.E. Macon, J.M. Leech, L.A. Kalekar, et al. 2021. Regulatory T cells promote innate inflammation after skin barrier breach via TGF-β activation. *Sci. Immunol.* 6:eabg2329. https://doi.org/10.1126/sciimmunol.abg2329

Myles, I.A., N.J. Earland, E.D. Anderson, I.N. Moore, M.D. Kieh, K.W. Williams, A. Saleem, N.M. Fontecilla, P.A. Welch, D.A. Darnell, et al. 2018. First-in-human topical microbiome transplantation with *Roseomonas mucosa* for atopic dermatitis. *JCI Insight*. 3:120608. https://doi.org/10.1172/jci.insight.120608

Nault, R., A.L. Forgacs, E. Dere, and T.R. Zacharewski. 2013. Comparisons of differential gene expression elicited by TCDD, PCB126, βNF, or ICZ in mouse hepatoma Hepa1c1c7 cells and C57BL/6 mouse liver. *Toxicol. Lett.* 223:52–59. https://doi.org/10.1016/j.toxlet.2013.08.013

Oboki, K., T. Ohno, N. Kajiwara, K. Arae, H. Morita, A. Ishii, T. Nambu, T. Abe, H. Kiyonari, K. Matsumoto, et al. 2010. IL-33 is a crucial amplifier of innate rather than acquired immunity. *Proc. Natl. Acad. Sci. USA*. 107: 18581–18586. https://doi.org/10.1073/pnas.1003059107

Oh, J., A.L. Byrd, C. Deming, S. Conlan, NISC Comparative Sequencing Program, H.H. Kong, and J.A. Segre. 2014. Biogeography and individuality shape function in the human skin metagenome. *Nature*. 514:59–64. https://doi.org/10.1038/nature13786

Paller, A.S., H.H. Kong, P. Seed, S. Naik, T.C. Scharschmidt, R.L. Gallo, T. Luger, and A.D. Irvine. 2019. The microbiome in patients with atopic dermatitis. *J. Allergy Clin. Immunol.* 143:26–35. https://doi.org/10.1016/j.jaci.2018.11.015

Peng, C., S. Zhang, L. Lei, X. Zhang, X. Jia, Z. Luo, X. Huang, Y. Kuang, W. Zeng, J. Su, and X. Chen. 2017. Epidermal CD147 expression plays a key role in IL-22-induced psoriatic dermatitis. *Sci. Rep.* 7:44172. https://doi.org/10.1038/srep44172

Ramasamy, S., E. Barnard, T.L. Dawson, and H. Li. 2019. The role of the skin microbiota in acne pathophysiology. *Br. J. Dermatol.* 181:691–699. https://doi.org/10.1111/bjd.18230

Rooks, M.G., and W.S. Garrett. 2016. Gut microbiota, metabolites and host immunity. *Nat. Rev. Immunol.* 16:341–352. https://doi.org/10.1038/nri.2016.42

Sanford, J.A., L.-J. Zhang, M.R. Williams, J.A. Gangoiti, C.-M. Huang, and R.L. Gallo. 2016. Inhibition of HDAC8 and HDAC9 by microbial short-chain fatty acids breaks immune tolerance of the epidermis to TLR ligands. *Sci. Immunol.* 1:eaah4609. https://doi.org/10.1126/sciimmunol.aah4609

Savinko, T., S. Matikainen, U. Saarialho-Kere, M. Lehto, G. Wang, S. Lehtimäki, P. Karisola, T. Reunala, H. Wolff, A. Lauerma, and H. Alenius. 2012. IL-33 and ST2 in atopic dermatitis: Expression profiles and modulation by triggering factors. *J. Invest. Dermatol.* 132:1392–1400. https://doi.org/10.1038/jid.2011.446

Schiering, C., T. Krausgruber, A. Chomka, A. Fröhlich, K. Adelmann, E.A. Wohlfert, J. Pott, T. Griseri, J. Bollrath, A.N. Hegazy, et al. 2014. The alarmin IL-33 promotes regulatory T-cell function in the intestine. *Nature*. 513:564–568. https://doi.org/10.1038/nature13577

Schmitz, J., A. Owyang, E. Oldham, Y. Song, E. Murphy, T.K. McClanahan, G. Zurawski, M. Moshrefi, J. Qin, X. Li, et al. 2005. IL-33, an interleukin-1-like cytokine that signals via the IL-1 receptor-related protein ST2 and induces T helper type 2-associated cytokines. *Immunity*. 23:479–490. https://doi.org/10.1016/j.immuni.2005.09.015

Schwarz, A., A. Bruhs, and T. Schwarz. 2017. The short-chain fatty acid sodium butyrate functions as a regulator of the skin immune system. *J. Invest. Dermatol.* 137:855–864. https://doi.org/10.1016/j.jid.2016.11.014

Shapiro, H., C.A. Thaiss, M. Levy, and E. Elinav. 2014. The cross talk between microbiota and the immune system: Metabolites take center stage. *Curr. Opin. Immunol.* 30:54–62. https://doi.org/10.1016/j.coi.2014.07.003

Shi, V.Y., M. Leo, L. Hassoun, D.S. Chahal, H.I. Maibach, and R.K. Sivamani. 2015. Role of sebaceous glands in inflammatory dermatoses. *J. Am. Acad. Dermatol.* 73:856–863. https://doi.org/10.1016/j.jaad.2015.08.015

Shinde, R., and T.L. McGaha. 2018. The aryl hydrocarbon receptor: Connecting immunity to the microenvironment. *Trends Immunol.* 39: 1005–1020. https://doi.org/10.1016/j.it.2018.10.010

Shu, M., Y. Wang, J. Yu, S. Kuo, A. Coda, Y. Jiang, R.L. Gallo, and C.M. Huang. 2013. Fermentation of *Propionibacterium acnes*, a commensal bacterium in the human skin microbiome, as skin probiotics against methicillin-resistant *Staphylococcus aureus*. *PLoS One*. 8:e55380. https://doi.org/10.1371/journal.pone.0055380

Silva, L.G., B.S. Ferguson, A.S. Avila, and A.P. Faciola. 2018. Sodium propionate and sodium butyrate effects on histone deacetylase (HDAC) activity, histone acetylation, and inflammatory gene expression in bovine mammary epithelial cells. *J. Anim. Sci.* 96:5244–5252. https://doi.org/10.1093/jas/sky373

Singh, N., A. Gurav, S. Sivaprakasam, E. Brady, R. Padia, H. Shi, M. Thangaraju, P.D. Prasad, S. Manicassamy, D.H. Munn, et al. 2014. Activation of Gpr109a, receptor for niacin and the commensal metabolite butyrate, suppresses colonic inflammation and carcinogenesis. *Immunity*. 40: 128–139. https://doi.org/10.1016/j.immuni.2013.12.007

Soshilov, A., and M.S. Denison. 2008. Role of the Per/Arnt/Sim domains in ligand-dependent transformation of the aryl hydrocarbon receptor. *J. Biol. Chem.* 283:32995–33005. https://doi.org/10.1074/jbc.M802414200

Stockinger, B., P. Di Meglio, M. Gialitakis, and J.H. Duarte. 2014. The aryl hydrocarbon receptor: Multitasking in the immune system. *Annu. Rev. Immunol.* 32:403–432. https://doi.org/10.1146/annurev-immunol-032713-120245

Sung, Y.Y., S.H. Kim, W.K. Yang, Y.C. Park, and H.K. Kim. 2018. Bleomycin aggravates atopic dermatitis via lung inflammation in 2, 4-dinitrochlorobenzene-induced NC/Nga mice. *Front. Pharmacol.* 9:578. https://doi.org/10.3389/fphar.2018.00578

Tang, W., S.G. Smith, W. Du, A. Gugilla, J. Du, J.P. Oliveria, K. Howie, B.M. Salter, G.M. Gauvreau, P.M. O'Byrne, and R. Sehmi. 2018. Interleukin-25 and eosinophils progenitor cell mobilization in allergic asthma. *Clin. Transl. Allergy*. 8:5. https://doi.org/10.1186/s13601-018-0190-2

Townsend, M.J., P.G. Fallon, D.J. Matthews, H.E. Jolin, and A.N. McKenzie. 2000. T1/ST2-Deficient mice demonstrate the importance of T1/ST2 in developing primary T helper cell type 2 responses. *J. Exp. Med.* 191: 1069–1076. https://doi.org/10.1084/jem.191.6.1069

Toyama, S., C.S. Moniaga, S. Nakae, M. Kurosawa, H. Ogawa, M. Tominaga, and K. Takamori. 2021. Regulatory T cells exhibit interleukin-33-dependent migratory behavior during skin barrier disruption. *Int. J. Mol. Sci.* 22:7443. https://doi.org/10.3390/ijms22147443

Vinolo, M.A.R., H.G. Rodrigues, E. Hatanaka, F.T. Sato, S.C. Sampaio, and R. Curi. 2011. Suppressive effect of short-chain fatty acids on production of proinflammatory mediators by neutrophils. *J. Nutr. Biochem.* 22: 849–855. https://doi.org/10.1016/j.jnutbio.2010.07.009

Wang, B., A. Morinobu, M. Horiuchi, J. Liu, and S. Kumagai. 2008. Butyrate inhibits functional differentiation of human monocyte-derived dendritic cells. *Cell. Immunol.* 253:54–58. https://doi.org/10.1016/j.cellimm.2008.04.016

Wang, W., N. Lv, S. Zhang, G. Shui, H. Qian, J. Zhang, Y. Chen, J. Ye, Y. Xie, Y. Shen, et al. 2012. Cidea is an essential transcriptional coactivator regulating mammary gland secretion of milk lipids. *Nat. Med.* 18:235–243. https://doi.org/10.1038/nm.2614

Wang, Y., A. Dai, S. Huang, S. Kuo, M. Shu, C.P. Tapia, J. Yu, A. Two, H. Zhang, R.L. Gallo, and C.M. Huang. 2014. Propionic acid and its esterified derivative suppress the growth of methicillin-resistant staphylococcus aureus USA300. *Benef. Microbes*. 5:161–168. https://doi.org/10.3920/BM2013.0031

Weidinger, S., and N. Novak. 2016. Atopic dermatitis. *Lancet*. 387:1109–1122. https://doi.org/10.1016/S0140-6736(15)00149-X

Werfel, T., J.P. Allam, T. Biedermann, K. Eyerich, S. Gilles, E. Guttman-Yassky, W. Hoetzenecker, E. Knol, H.U. Simon, A. Wollenberg, et al. 2016. Cellular and molecular immunologic mechanisms in patients with atopic dermatitis. *J. Allergy Clin. Immunol.* 138:336–349. https://doi.org/10.1016/j.jaci.2016.06.010

Williams, H.C., P.G. Burney, R.J. Hay, C.B. Archer, M.J. Shipley, J.J. Hunter, E.A. Bingham, A.Y. Finlay, A.C. Pembroke, R.A. Graham-Brown, et al. 1994. The U.K. Working Party's Diagnostic Criteria for Atopic Dermatitis. I. Derivation of a minimum set of discriminators for atopic dermatitis. *Br. J. Dermatol.* 131:383–396. https://doi.org/10.1111/j.1365-2133.1994.tb08530.x

Yamazaki, Y., Y. Nakamura, and G. Núñez. 2017. Role of the microbiota in skin immunity and atopic dermatitis. *Allergol. Int.* 66:539–544. https://doi.org/10.1016/j.alit.2017.08.004

Yang, W., T. Yu, X. Huang, A.J. Bilotta, L. Xu, Y. Lu, J. Sun, F. Pan, J. Zhou, W. Zhang, et al. 2020. Intestinal microbiota-derived short-chain fatty acids regulation of immune cell IL-22 production and gut immunity. *Nat. Commun.* 11:4457. https://doi.org/10.1038/s41467-020-18262-6

Youn, S.H., C.W. Choi, J.W. Choi, and S.W. Youn. 2013. The skin surface pH and its different influence on the development of acne lesion according to gender and age. *Skin Res. Technol.* 19:131–136. https://doi.org/10.1111/srt.12023

Yu, J., Y. Luo, Z. Zhu, Y. Zhou, L. Sun, J. Gao, J. Sun, G. Wang, X. Yao, and W. Li. 2019. A tryptophan metabolite of the skin microbiota attenuates inflammation in patients with atopic dermatitis through the aryl hydrocarbon receptor. *J. Allergy Clin. Immunol.* 143:2108–2119.e12. https://doi.org/10.1016/j.jaci.2018.11.036

Zeng, F., H. Chen, L. Chen, J. Mao, S. Cai, Y. Xiao, J. Li, J. Shi, B. Li, Y. Xu, et al. 2021. An autocrine circuit of IL-33 in keratinocytes is involved in the progression of psoriasis. *J. Invest. Dermatol.* 141:596–606.e7. https://doi.org/10.1016/j.jid.2020.07.027

Zhang, S., C. Rowlands, and S. Safe. 2008. Ligand-dependent interactions of the Ah receptor with coactivators in a mammalian two-hybrid assay. *Toxicol. Appl. Pharmacol.* 227:196–206. https://doi.org/10.1016/j.taap.2007.10.019

Zhang, S., G. Shui, G. Wang, C. Wang, S. Sun, C.C. Zouboulis, R. Xiao, J. Ye, W. Li, and P. Li. 2014. Cidea control of lipid storage and secretion in mouse and human sebaceous glands. *Mol. Cell. Biol.* 34:1827–1838. https://doi.org/10.1128/MCB.01723-13

Zhou, L., M. Shi, L. Zhao, Z. Lin, Z. Tang, H. Sun, T. Chen, Z. Lv, J. Xu, Y. Huang, and X. Yu. 2017. Clonorchis sinensis lysophospholipase a upregulates IL-25 expression in macrophages as a potential pathway to liver fibrosis. *Parasit. Vectors*. 10:295. https://doi.org/10.1186/s13071-017-2228-z
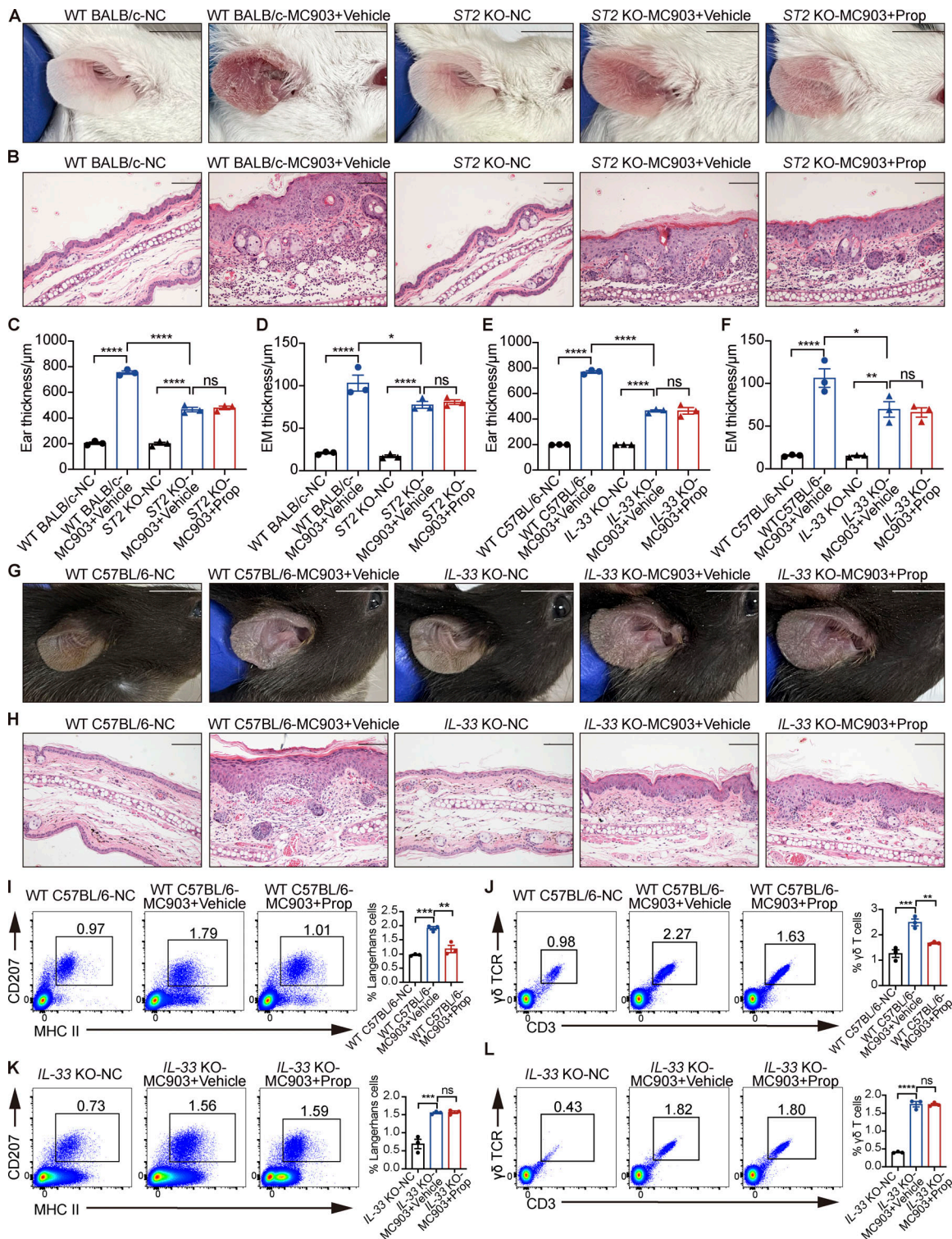
Figure S1. **The absence of IL-33 or ST2 abolishes the propionate-mediated attenuation in skin inflammation of the MC903-treated mice. (A–D)** MC903 or MC903 plus propionate (Prop)/vehicle was applied topically on the ears of WT BALB/c mice and *ST2* KO mice once daily for 9 d (*n* = 3 per group). Representative gross appearance (A), H&E staining of ear sections on day 9 (B), ear thickness (C), and epidermal (EM) thickness of ear sections under high-power magnification (D) of each mice group are shown. **(E–L)** MC903 or MC903 plus propionate/vehicle was applied topically on the ears of WT C57BL/6 mice and *IL-33* KO mice once daily for 14 d (*n* = 3 per group). Ear thickness (E), epidermal thickness of ear sections under high-power magnification (F), representative gross appearance (G), and H&E staining of ear sections on day 14 (H) of each mice group are shown. Representative flow cytometry dot plots of LCs (I and K) and γδ T cells (J and L) in ears of each mice group are shown. Bar graphs on the right showing the percentage of LCs/γδ T cells within MHC II⁺ CD207⁺ gates (LCs) or CD3⁺ γδ TCR⁺ gates (γδ T cells). Scale bar = 1 cm (A and G); 100 μm (B and H). Data are representative of three independent experiments and are expressed as means ± SEM. Statistical significance was analyzed by one-way ANOVA followed by Tukey's test. *, P < 0.05; **, P < 0.01; ***, P < 0.001; ****, P < 0.0001.
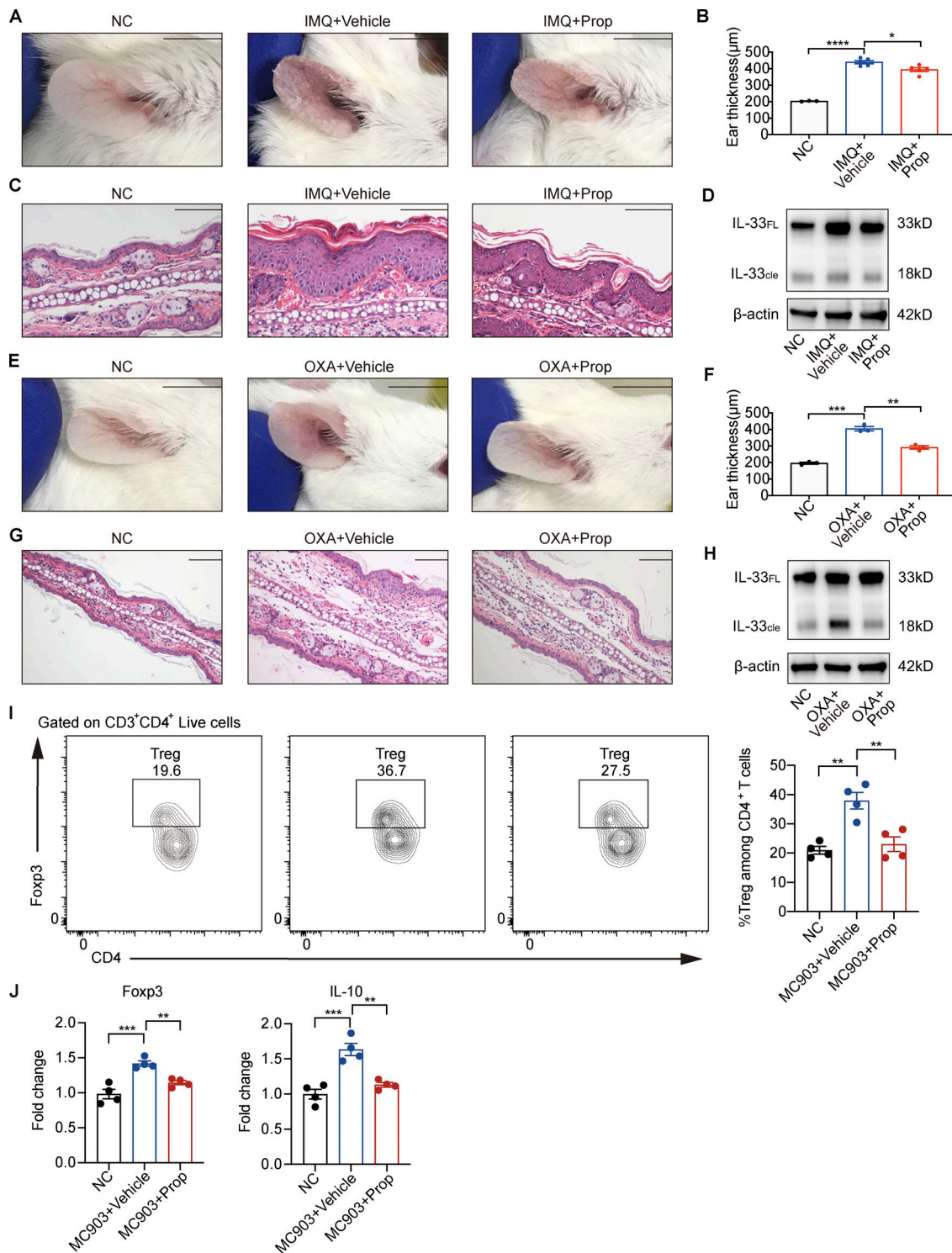
Figure S2. **Topical propionate treatment attenuates IMQ-, OXA-, or MC903-induced skin inflammation in mice. (A–D)** IMQ-induced psoriatic dermatitis was produced in the ears of mice, following which the animals were topically treated with propionate once daily for 14 d (n = 3–5 per group). Gross appearance of the ears (A), ear thickness (B), H&E staining of ear sections (C), and the protein expression of IL-33 in lesional ears (D) are shown. **(E–H)** The mouse model of contact hypersensitivity was generated using OXA, after which propionate was topically applied during the sensitization and challenge stages (n = 3 per group). Gross appearance of the ears (E), ear thickness (F), H&E staining of ear sections (G), and the protein expression of IL-33 in lesional ears (H) are shown. **(I and J)** MC903 or MC903 plus propionate (Prop)/vehicle was applied topically on the ears of WT BALB/c mice once daily for 9 d (n = 4 per group). **(I)** Representative flow cytometry dot plots of Tregs in ears of each mice group gated on $CD3^+$ $CD4^+$ live cells. Bar graphs on the right showing the percentage of Tregs within $CD3^+$ $CD4^+$ $Foxp3^+$ gates among $CD4^+$ T cells. **(J)** The mRNA expression of Foxp3 and IL-10 in the ears of mice in each group. IL-33$_{FL}$, the full-length form of IL-33; IL-33$_{cle}$, the cleaved form of IL-33. Scale bar = 1 cm (A and E); 100 μm (C and G). Data are representative of three independent experiments and are expressed as means ± SEM. Statistical significance was analyzed by one-way ANOVA followed by Tukey's test. *, $P < 0.05$; **, $P < 0.01$; ***, $P < 0.001$; ****, $P < 0.0001$. Source data are available for this figure: SourceData FS2.
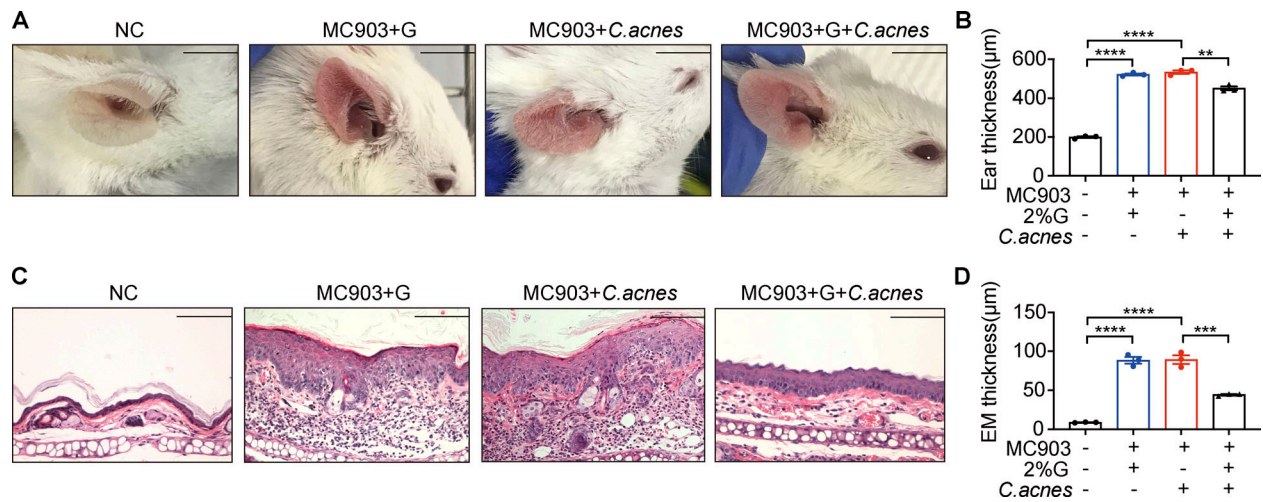
Figure S3. **Lipophilic microbes in lipid-rich conditions attenuate MC903-induced AD-like dermatitis in mice.** *C. acnes* (1×10^5 CFUs/ml) mixed with 2% glycerol (G) were topically applied onto MC903-treated mouse ears once daily for 9 consecutive days (*n* = 3 per group). **(A)** Gross appearance of the ears. **(B)** Ear thickness of mice. **(C)** H&E staining of ear sections. Scale bar = 100 µm. **(D)** Epidermal (EM) thickness of ear sections. Scale bar = 1 cm (A); 100 µm (C). Data are representative of three independent experiments and are expressed as means ± SEM. Statistical significance was analyzed by one-way ANOVA followed by Tukey's test. **, $P < 0.01$; ***, $P < 0.001$; ****, $P < 0.0001$.
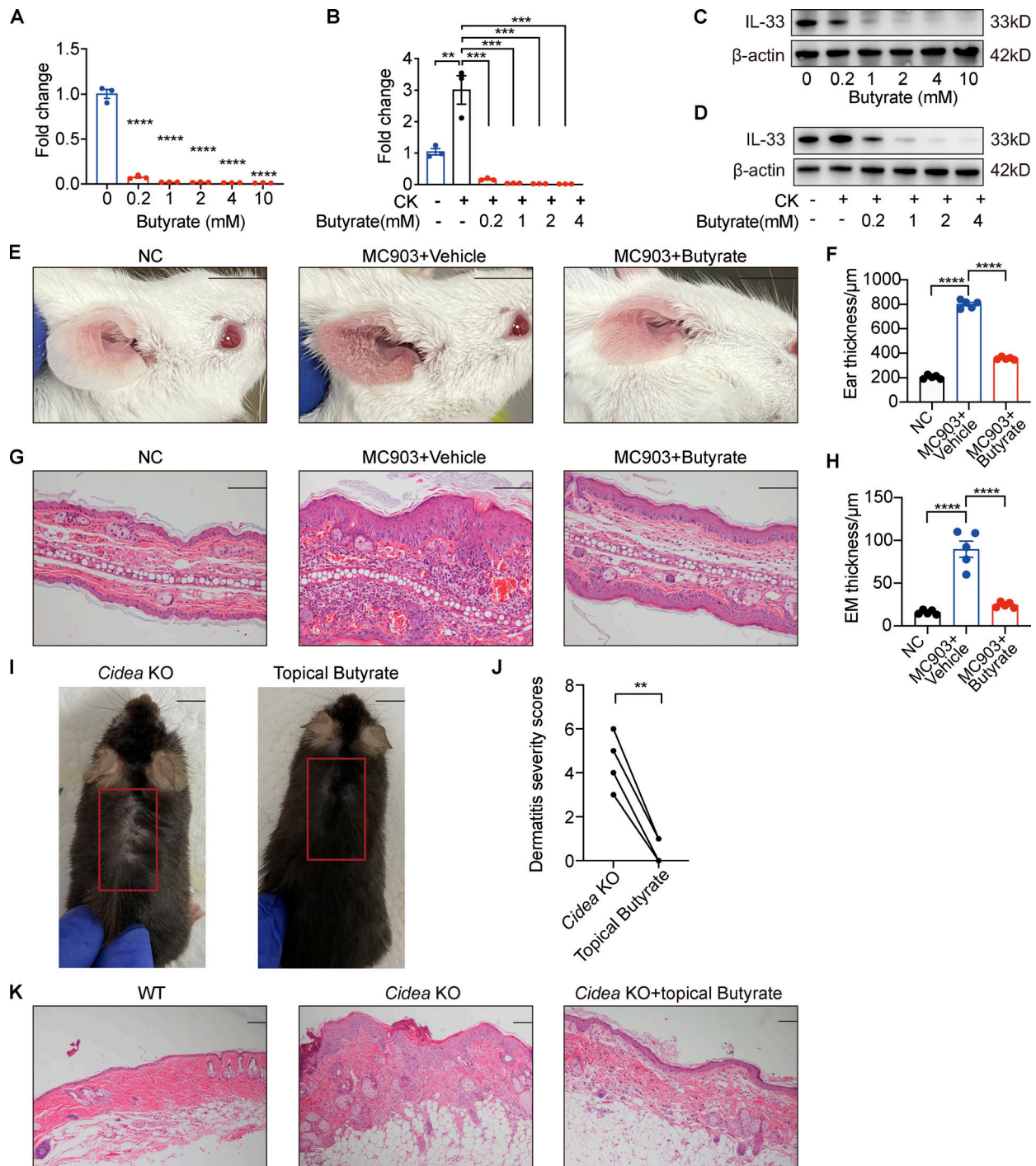
Figure S4.   **Butyrate suppresses IL-33 expression in keratinocytes and inhibits skin inflammation of AD mouse model. (A–D)** IL-33 mRNA and protein expression in keratinocytes treated with different concentrations of butyrate (0.2–10 mM) in standard culture medium or supplemented with IL-4 and IL-1α for 24 h (n = 3 per group). **(E–H)** MC903 or MC903 plus butyrate (1 mM)/vehicle was applied topically on the ears of BALB/c mice once daily for 9 d (n = 5 per group). **(E)** Representative gross appearance of the ears. **(F)** Ear thickness of the mice in each group. **(G)** H&E staining of ear sections. **(H)** Epidermal (EM) thickness of ear sections under high-power magnification. **(I–K)** *Cidea* KO mice were topically applied with butyrate (1 mM) on the lesional skin twice daily for 21 d (n = 4 per group). **(I)** Gross appearance of skin lesions in *Cidea* KO mice before and after topical butyrate treatment. The red box indicates the skin lesions treated with butyrate. **(J)** Severity scores of skin lesions in *Cidea* KO mice before and after butyrate treatment. **(K)** H&E staining of skin samples from WT mice, lesional skin of *Cidea* KO mice, and lesional skin of *Cidea* KO mice treated with butyrate. Scale bar = 1 cm (E and I); 100 µm (G and K). Data are representative of three independent experiments and are expressed as means ± SEM. Statistical significance was analyzed by one-way ANOVA followed by Dunnett's test (A and B) and paired t test (J). *, $P < 0.05$; **, $P < 0.01$; ***, $P < 0.001$; ****, $P < 0.0001$. Source data are available for this figure: SourceData FS4.
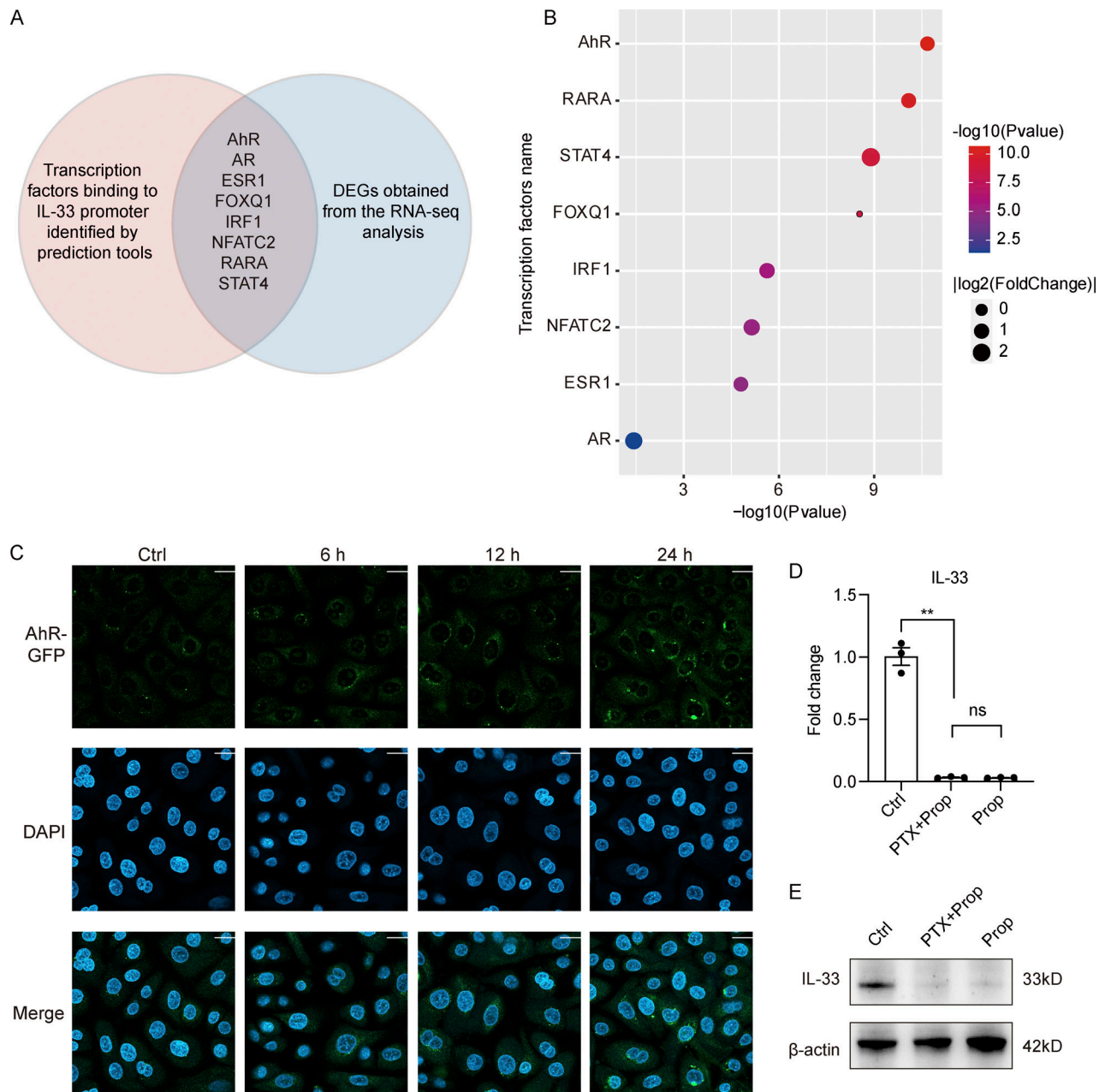
Figure S5. **Mechanism for the inhibitory effect of propionate on IL-33 expression. (A and B)** Analysis of potential transcription factors binding to *IL-33* promoter. **(A)** The Venn diagram of intersection between transcription factors predicted to bind *IL-33* promoter and DEGs obtained from the RNA-seq analysis. The red circle represents transcription factors predicted by PROMO database (http://alggen.lsi.upc.es/cgi-bin/promo_v3/promo/promoinit.cgi?dirDB=TF_8.3) and further verified by the online software LASAGNA-search 2.0 (https://biogrid-lasagna.engr.uconn.edu/lasagna_search/). The blue circle represents DEGs (| fold-change| >1.5 versus control, P < 0.05) obtained from the RNA-seq analysis. The intersection lists transcription factors that exist in both circles. **(B)** The bubble chart showing P values and fold-change of the listed transcription factors. **(C)** Representative confocal images showing the localization of AhR in keratinocytes treated with CH-223191 for 1 h before stimulation with propionate (4 mM) for different times. Scale bar = 20 μm. **(D and E)** Keratinocytes were treated with PTX (0.2 μg/ml) for 1 h before stimulation with propionate (Prop; 4 mM) for 24 h. Results of RT-qPCR analysis (D) and Western blotting analysis (E) for the expression of IL-33 in keratinocytes are shown. Data are representative of three independent experiments and are expressed as means ± SEM. Statistical significance was analyzed by one-way ANOVA followed by Tukey's test. **, P < 0.01. Source data are available for this figure: SourceData FS5.

Provided online is Table S1. Table S1 lists primers for RT-qPCR analysis and ChIP assay.

Qiu et al.   **Journal of Experimental Medicine**   S6
Sebum–propionate–IL-33 axis in atopic dermatitis   https://doi.org/10.1084/jem.20212397